Offshore wind resource assessment using synthetic aperture radar and meteorological mesoscale model

Takeyama, Yuko

(Degree)
博士（工学）

(Date of Degree)
2013-09-25

(Date of Publication)
2014-09-01

(Resource Type)
doctoral thesis

(Report Number)
甲第5973号

(URL)
https://hdl.handle.net/20.500.14094/D1005973

Doctoral Dissertation

Offshore Wind Resource Assessment using Synthetic Aperture Radar and Meteorological Mesoscale Model

合成開口レーダと数値気象モデルによる洋上風力資源量評価

July 2013

平成 25 年 7 月

Graduate School of Maritime Sciences, Kobe University

神戸大学大学院海事科学研究科

Yuko Takeyama

竹山　優子

Acknowledgement

The doctoral dissertation has been completed with many supports of several people. I would like to express my gratitude to all of them.

First of all, I am extremely grateful to my supervisor Assoc. Prof. Dr. Teruo Ohsawa, Graduate School of Maritime Science, Kobe University, for his valuable guidance and scholarly inputs, which I have received throughout the research work since I started a master's course. He had always made himself available to reply to my demands and queries despite his busy schedules. I would like to continue to emulate his positive attitudes and research skills.

I thank Prof. Dr. Katsutoshi Kozai, Graduate School of Maritime Science, Kobe University, for the academic support to carry out the research work. He was a supervisor in my master's course and created a great opportunity for me to study about synthetic aperture radars. The master's thesis could be based on my research activities.

I also thank Headmaster Dr. Hiroshi Ishida, Oshima National Collage of Maritime Technology, and Prof. Dr. Eiichi Kobayashi, Graduate School of Maritime Science, Kobe University, for giving me meaningful comments.

All members of the Air-Sea Laboratory have been kind enough to extend their cooperation at various phases of the research work, whenever I approached them, especially, Mr. Kazunao Kanda and Mr. Tomohiro Yamashita. I am deeply grateful to Assoc. Prof. Dr. Mitsuru Hayashi, Kobe University Research Center for Inland Seas, for her valuable suggestions and concise comments. I am also grateful to Ms. Minako Tokura and Mr. Nobuo Nozaki for their sincere help. I do hereby acknowledge all of them.

Furthermore I would like to thank Dr. Charlotte Bay Hasager and Dr. Merete Badger, Technical University of Denmark (DTU), Department of Wind Energy, for their kindly help. I have no doubt that the experiences of my one year stay at DTU Risoe Campus will help my future work.

Finally, I thank my family for their support.

謝辞

本論文をまとめるにあたり，多くの方々の御協力を頂きました．全ての方に謝意を表します．

始めに，研究を進めるにあたり，御指導，御鞭撻を頂いた神戸大学海事科学研究科大澤輝夫准教授に心より感謝致します．大澤准教授には筆者が神戸大学自然科学研究科博士前期課程在学中より研究について基礎からご指導いただきました．また，いつでも研究に関する議論の場を設け，研究を継続する環境を整えて頂きました．学位取得へ導いていただいた事に深く感謝しております．今後も研究に取り組む姿勢を見習っていきたいと思います．

合成開口レーダに係る研究を始めるきっかけを下さり，また，人工衛星データの解析研究に関してご指導いただきました神戸大学海事科学研究科香西克俊教授に心より感謝申し上げます．指導教官として御指導いただいた修士論文は筆者の研究の基礎になっております．

審査において貴重なご助言を頂いた大島商船高等専門学石田廣史校長および神戸大学海事科学研究科小林英一教授に心より感謝申し上げます．

研究の解析にあたり尽力頂いた，神戸大学海事科学研究科山下智大学生，神田和直学生他，研究室の皆さんに感謝致します．

公私ともに数多くのご指導，ご協力をいただいた神戸大学自然科学系先端融合研究環内海域環境教育研究センター林美鶴准教授，海洋気象研究室戸倉美奈子事務補佐員，野崎信夫技術員に感謝申し上げます．

さらに，論文執筆に際し有意義な助言を頂き，また，博士課程最後の半年の研究活動をデンマーク工科大学 Risoe キャンパスにて実施する環境を提供下さったデンマーク工科大学 Dr. Charlotte Bay Hasager 上席研究員および Dr. Merete Badger 上席研究員に深く感謝いたします．デンマークにおける研究経験は，今後の研究活動の支えになると確信いたしております．

最後に，学位取得までの長い道のりを支えてくれた家族に感謝致します．

Abstract

This dissertation gives offshore wind field retrieval and offshore wind resource assessment in coastal waters by means of satellite-borne synthetic aperture radar (SAR) and meteorological mesoscale model. To acquire precise wind information for selection of suitable areas at relatively low cost, SAR and numerical meteorological models are well used in Europe, where large offshore wind farms are in operation. These methods have already been confirmed as effective in the open seas. However, there are still rooms for consideration in coastal waters, especially Japanese coastal waters, which have complex onshore terrains and unstable atmospheric conditions due to prevailing monsoon winds and warm Kuroshio currents flowed strongly along the north western Pacific Ocean. In this dissertation, the both methods for the sea surface wind field retrieval are evaluated and improved in Japanese coastal waters with ENVISAT ASAR images and the Weather Research and Forecasting model (WRF), and then the wind resource maps are made with the retrieved wind fields by the improved methods. Contents of each chapter are summarized as follows.

In Chapter 1, backgrounds, reviews of previous studies on sea surface wind retrieval and purposes of this dissertation are described. A renewable energy resource had been generally expected to be a solution for problems of the global warming and low self-sufficiency of energy supply in Japan. Moreover, the renewable energy have been focused as secure and safety energy resources since The Fukushima Daiichi nuclear accident. Wind power generation have been had negative impressions in Japan because of a health hazard by low frequency waves and uncertainty for a structurally strength of turbines, which are serious problems for inhabitants living close to a wind farm. But now, wind farms tend to spread to offshore areas. We focus on new problems related to the offshore wind resource assessment though these previous problems can be ignored on offshore areas. A wind condition is one of the most important information for the wind resources assessment when a large wind farm is established. There are few reports concerning the wind speed retrieval in coastal waters using SAR images, though there are still some validation studies in open waters. In coastal waters, an effect from land should be considered for the wind speed retrieval. Moreover, the SAR-retrieved

wind speed can be affected by an atmospheric stability because SAR retrieves the wind speed based on the observation of sea surface roughness using active microwaves. Japanese coastal waters are one of the most unstable atmospheric condition areas, and it is necessary to examine these effects in the retrieved wind speed. Some geophysical model functions (GMFs), which are used for the wind speed retrieval from SAR images, have been still developed both with and without the consideration of the atmospheric stability. These GMFs and the effect of the atmospheric stability are discussed in Chapter 2. Meanwhile, these GMFs require inputs as wind directions. An effectiveness of weather research and forecasting (WRF) model simulated wind directions, which can be acquired with higher spatial resolutions and few missing values, is examined in Chapter 3. Finally, the wind resources assessment is carried out at Shirahama using these discussed methods in Chapter 4.

In Chapter 2, the dissertation discussed the accuracies of GMFs for retrieval of sea surface wind speed from satellite-borne SAR images in Japanese coastal waters characterized by short fetches and variable atmospheric stability conditions. *In-situ* observations from two validation sites, Hiratsuka and Shirahama, are used for comparison of the retrieved sea surface wind speeds using CMOD (C-band model) 4, CMOD_IFR2, CMOD5 and CMOD5.N. Of all the GMFs, the latest C-band GMF, CMOD5.N, has the smallest bias and root mean square error (RMSE) at both sites. All of the GMFs exhibit a negative bias in the retrieved wind speed. In order to understand the reason for this bias, all SAR-retrieved wind speeds are separated into two categories: onshore wind (blowing from sea to land) and offshore wind (blowing from land to sea). Only offshore winds were found to exhibit the large negative bias, and short fetches from the coastline may be a possible reason for the negative biases. Moreover, it is clarified that in both the unstable and stable conditions, CMOD5.N has atmospheric stability effectiveness, and can keep the same accuracy with CMOD5 in the neutral condition. In short, at the moment, CMOD5.N is thought to be the most promising GMF for the SAR wind speed retrieval with the atmospheric stability correction in Japanese coastal waters.

In Chapter 3, effectiveness of the WRF wind direction as input to GMF for the sea surface wind speed retrieval from SAR images is examined with CMOD5.N, which is confirmed its effectiveness in Chapter 2. In order to validate the effectiveness of this

approach, the accuracies of the SAR-retrieved wind speed with the WRF wind direction are compared with those calculated using three other external sources of wind directions; meso-analysis of the Japan Meteorological Agency (MANAL), the SeaWinds microwave scatterometer on QuikSCAT, and National Center for Environmental Prediction/National Center for Atmospheric Research final analysis using operational global analysis data (NCEP FNL). In the result of this validation, it is shown that the SAR-retrieved wind speed with the WRF wind direction does not have the highest accuracy, though the WRF wind direction itself has the highest accuracy of the other external wind directions. In the next step, these comparisons are carried out using only onshore winds for elimination of the effect of the short fetch, which is described in Chapter 2. In this comparison, RMSE on wind speed with the WRF wind direction is the smallest of all wind directions, and the uncertainty is 1 m/s at the 95% confidence level of RMSE. This result shows that WRF-simulated wind direction is the most previous inputs for GMFs.

In Chapter 4, offshore wind resource maps for the coastal waters off Shirahama, Japan, were made based on 104 images of the ENVISAT satellite. Wind speed fields were derived from the SAR images with the latest GMF, CMOD5.N with WRF simulated wind directions. From the retrieved wind speeds, mean wind speed and energy density were estimated by means of the Weibull distribution function. Their accuracy was examined in comparison with *In-situ* measurements from the Shirahama offshore platform and the South Wakayama buoy (SW-buoy). It was found that the SAR-derived 10 m-height wind speed had a bias of 0.52 m/s and a RMSE of 2.33 m/s at Shirahama. It was also found that the mean wind speeds estimated from SAR images and the Weibull distribution function were overestimated at both sites. The ratio between SAR-derived and *In-situ* measured mean wind speeds is 1.07 (Shirahama) and 1.23 (SW-buoy), and these ratios were used for a long-term bias correction in the SAR-derived wind speed. Finally, mean wind speed and wind energy density maps at 80 m height were made based on the corrected SAR-derived 10 m-height wind speeds and the ratios U80/U10 calculated from the mesoscale meteorological model WRF.

In Chapter 5, general conclusions of this dissertation and issues in the future are described. Future works are necessary for the investigation into the effect of the short fetch, causing a negative bias. This negative bias could be more serious in coastal

waters than the error originating from wind direction and GMF. Many factors contribute to a sea surface roughness, and these factors can be affected each other intricately. Many kinds of SAR images with different observation modes should be attempted for next study, in order to clear the effect of the short fetch. Additionally, more number of SAR images may lead more accurate distributions of the mean wind speed and energy density.

要旨

本論文は人工衛星に搭載された合成開口レーダ(SAR)および数値気象モデルを用いた海上風推定と洋上風力発電の資源量評価手法について述べるものである. 既に大型風力発電所を運用している欧州では, 比較的安価に風況および資源量評価を行う手段としてSARとメソ気象モデルが実用化され, 外洋におけるこれらの手法についての精度評価も既に実施されている. しかし, 複雑な海岸地形を有し, かつ, 卓越する季節風と太平洋に沿って流れる黒潮暖流によって不安定な大気状態である日本沿岸域においては, 検証が十分とは言えない. そこで, 本論文では ENVISAT 衛星搭載の SAR 画像とメソ気象モデル(WRF)を用い, 日本沿岸域における風況推定に必要な手法の検証および開発を行う. その後, この検証・開発した手法から推定された風速および風向情報を用いて風力資源量推定を行い, その分布図を作成する. 以下に各章の内容をまとめる.

第一章は序章として研究背景, 海上風速および風向推定の既存研究調査, および本論文の研究目的を述べる. これまで, 再生可能エネルギーは地球温暖化や日本の低いエネルギー自給率問題の解の一つとして期待されてきた. また, 福島第一原子力発電所の事故以来, 安全なエネルギー源の一つとしても注目されている. 過去, 日本では, 周辺住民からの低周波による人体への影響や構造上の強度に対する不信感があり, 風力発電について否定的な評価をされることがあった. しかし, 現在, 風力発電は陸上から洋上へ移行しつつある. これにともない, 我々は旧来の問題から新たな洋上風況把握ついての問題に対峙している. 風力発電において, 風車設置に必要な風況は最も重要な情報の一つである. 欧州では既にSARを用いた海上風推定が実施され, その検証結果もいくつか存在するが, これらは外洋における研究が中心であり, 陸の影響を受ける可能性の高い沿岸域における検証は少ない. また, 沿岸域は陸域の影響を大きく受ける. さらに, SAR は風の直接観測ではなくマイクロ波による海面の間接的な観測を行っているため, 大気安定度が風速の推定精度に影響を与える可能性がある. 日本沿岸域は世界でも有数の大気状態が不安定な特殊海域であり, これらが風速の推定精度に与える影響を検証する必要がある. SAR による海上風推定で用いられるモデル関数(GMF)は既にいくつか開発されているが, 大気安定度の考慮については対応が分かれている. 第二章では日本沿岸域を観測したSAR画像から複数のGMFを用いて推定した海上風の検証を行い, 大気安定度がSAR風速推定精度に与える影響明らかにするとともに, 日本沿岸域に適した GMF の選定と大気安定

度補正方法の開発を行う. 一方で, SAR による海上風推定で用いる GMF は風速算出の際に風向の情報を必要とする. 第三章では安定した風向情報の取得が可能な数値気象モデル WRF の算出風向を GMF の入力値とする手法を試みる. WRF 風向の比較データとして, 他の利用可能な複数の風向情報を用い, GMF の風向依存性を明らかにし, WRF 風向の GMF への利用可能性について検討を行う. 第四章では, 第二章, 第三章で検証・開発された手法を用い, 和歌山県白浜沖における風力資源量の推定とその分布図の作成を行う.

第二章では, 陸域に近く, 大気状態が変化しやすい日本沿岸域において, SAR 画像から複数の GMF を用いた風速の推定精度検証を実施した. 対象海域である神奈川県平塚と和歌山県白浜で観測された実測値は4つの GMF である CMOD4, CMOD_IFR2, CMOD5 および CMOD5.N から算出された風速の検証用として使用した. 検証の結果, これらの GMF のうち, 最新のモデルである CMOD5.N は両海域において最も小さな平均誤差と最小二乗誤差を示した. また, 全ての GMF によって算出された風速は実測値に対して過小評価傾向となった. この過小評価の原因を調べるため, 全ての風向を onshore (海から陸への風) と offshore (陸から海への風) に分類したところ, offshore 時にのみこの過小評価傾向が強く表れることが分かり, 過小評価傾向が陸からの吹送距離 (フェッチ) の短さにある可能性が高いことが分かった. 一方, 大気安定度について安定, 中立および不安定な時に分けた場合, 中立の時には大気安定度を考慮していない CMOD5 と大気安定度の影響を考慮している CMOD5.N はほぼ同じ風速推定精度であったが, 安定および不安定な時には CMOD5.N の方が高い精度を示し, CMOD5.N が日本沿岸域における大気安定度の補正に有効であることが分かった.

第三章では, 第二章にてその効果が示された CMOD5.N を用いて, この CMOD5.N に入力値として必要となる風向情報として, WRF によって算出された風向の有効性を検証した. この検証のため, WRF 風向を用いて算出された SAR 風速は他に入手可能な風向情報, 気象庁メソ客観解析値(MANAL), マイクロ波散乱計(QuikSCAT)およびアメリカ国立環境予測センター再解析データ(NCEP FNL)を用いた時の SAR 風速との比較検証を行った. 検証の結果, 4つの風向のうち, WRF 風向は高い空間分解能で風向を推定することが可能であり, かつ, 他の 3 つの風向よりも風向そのものの精度が高いにもかかわらず, 他の風向よりも高い精度で風速を推定しない結果となった. この理論に合わない結果の要因について, 第二章でも問題となった短い吹送距離による陸の影響が疑われた. この影響を取り除くため, 検証対象データを

onshore に絞り，再度 4 つの風向を用いた検証を実施した．この結果，WRF 風向を入力した SAR 推定風速が最も小さな RMSE を示した．さらに，WRF 風向を入力値とした SAR 推定風速の RMSE の 95%信頼区間は 1 m/s 以下となり，他の風向の信頼区間よりも明らかに狭く，小さい値を示すことが分かった．Onshore の風に限定したことで検証のサンプル数は小さくなったが，95%信頼区間によりこの検証の信頼性が示され，WRF の風向情報が SAR による風速推定に有効であることがわかった．

第四章では，ENVISAT ASAR 104 シーンを用いて，白浜沿岸域を対象とした風力資源量マップの作成を実施した．第二章および第三章で検証を行った CMOD5.N および WRF 風向を用いて白浜沖における風速分布を求め，その後，得られた風速からワイブル分布関数を用いて平均風速および平均エネルギー分布を算出した．また，精度の検証用として，白浜観測鉄塔及び和歌山沖南西沖ブイの長期実観測風速データを使用した．検証の結果，SAR から推定された風速は白浜において 0.52m/s の平均誤差と 2.33m/s の最小二乗誤差を持ち，過大評価傾向にあることが分かった．また，この誤差により，ワイブル分布関数によって導かれた平均風速にも過大評価の傾向があることが分かった．この過大評価は長期現場風速の観測結果と比べて白浜において 1.07 倍，南西沖ブイにおいて 1.23 倍という結果であった．最終的に精度の高いエネルギー密度分布図を作成するため，これら SAR 平均風速と長期現場平均風速の比率を使って SAR 平均風速の補正を行い，10m高度における平均風速とエネルギー密度分布図を作成した．また，その後，WRF から推定された 10m 高度風速と 80m 高度風速比を用いて風車ハブ高度にあたる 80m 高度の平均風速とエネルギー密度分布図の作成を実施した．

第五章では，本論文の全体総括と今後の課題について述べる．今後の課題として，沿岸域における短い吹送距離による陸の影響の補正手法の開発がある．海面の粗度には様々な大気現象が関係しており，さらにその大気現象自体も大気海洋相互作用によって影響されているため，陸の影響には非常に複雑な要因が関係していると予想できる．しかし，この陸の影響は SAR 海上風推定において無視できるものではない．この解決には，より多くの種類の異なった観測モードの SAR 画像を用いた解析を行う必要がある．また，風力資源量マップにはより多くの SAR 画像を適用することにより，さらに高精度なマップ作成が可能になると考える．これらは次の課題としたい．

Contents

Chapter 1

Introduction

1.1 Backgrounds

A development of renewable energy resources had been generally expected to be a solution for problems of the global warming and lower self-sufficiency of energy supply in Japan. As well as these existing problems, since the Fukushima Daiichi nuclear accident, which was a consequence of the 9.0 magnitude Tohoku earthquake and the following tsunami on March 11th, 2011, the renewable energy have been focused as secure and safety energy resources. The wind power generation, which is one of the renewable energy, has potential to become a part of main energy resources. Wind power generation had been had negative impressions in the past because of a health hazard by low frequency waves and uncertainty for a structurally strength of turbines, which are serious problems for inhabitants living close to a wind farm. But now, wind farms tend to spread to offshore areas. We focus on new problems related to the wind resource assessment though these previous problems can be ignored.

Wind conditions are one of the most important information for the installation of the large wind farm. An incorrectness of estimated wind speeds absolutely leads to a downfall of the wind farm. To acquire the wind speed with high accuracy at a lower cost, artificial satellites and numerical meteorological models are well used in Europe, where many offshore wind farms are in operation. These methods are confirmed as effective used for the accurate wind speed estimation in European sea waters. However, there are still rooms for consideration in Japanese coastal waters, which have complex onshore terrains and unstable atmospheric conditions due to prevailing monsoon winds and warm and cold ocean currents. These circumstances are remarkably difference from European coastal waters. Thus, it is necessary to validate the wind speed retrieved by the artificial satellites and the numerical meteorological model.

1.2 Sea surface wind speed retrieval

An estimation of sea surface wind vector has been attempted since the 1980s

using a microwave scatterometer and synthetic aperture radar (SAR). The scatterometer can retrieve the sea surface wind speed and direction with a horizontal resolution on the order of several dozen kilometers. However, because of its coarse horizontal resolution, the scatterometer cannot estimate accurate wind vectors close to land. Meanwhile, the SAR with a higher spatial resolution (e.g., 10 to 50 m) than the scatterometer has been used to retrieve the sea surface wind speed in coastal waters. In previous studies, the SAR-retrieved wind speeds have been found to contain root mean square errors (RMSEs) of 2 to 3 m/s in coastal waters (e.g., Horstmann *et al.*, 2000, Monaldo *et al.*, 2001) with a geophysical model functions (GMF), which is an empirical models to convert from intensity of backscattered microwaves to wind speed. Mainly, four major GMFs, CMOD4 (Stoffelen *et al*., 1997), CMOD5 (Hersbach *et al*., 2007), CMOD_IFR2 (Quilfen *et al*., 1998), and CMOD5.N (Hersbach, 2010) has been developed. There are few studies to validate these GMFs at onshore area, though most validations have been performed at least 10 km distant from the coastline (Lehner *et al*., 1998, Horstmann *et al*., 2002, Hasager *et al*., 2004). It has not been clarified which GMFs are promised to retrieve sea surface wind speed with higher accuracies in coastal waters.

On the other hand, the numerical meteorological model also has been used to estimate an accurate wind speed and direction. In the previous study, the Weather Research and Forecasting model (WRF) have been attempted to estimate the wind speed by Shimada *et al* (2011). in Japanese coastal waters, respectively. The simulated wind speeds by fifth-generation Penn State/National Center for Atmospheric Research (NCAR) mesoscale model (MM5) also validated with those by RADARSAT-1 SAR in Hiratsuka, Japan (Takeyama *et al*., 2006). In this study, it is reported that the SAR retrieved wind speed has higher accuracy than mesoscale model. Thus, in this dissertation, the SAR image is used for the sea surface wind speed retrieval.

1.3 Sea surface wind direction retrieval

Wind direction is indispensable to retrieve the sea surface wind speed using GMFs because the GMF describes the relationship among microwave backscatter, local incidence angle, relative wind direction, and wind speed at 10 m above mean sea level (MSL). The wind direction can be retrieve from both the SAR image itself and the numerical meteorological model. The Fourier transform has often been used for the detection of the wind direction from the SAR image itself (e.g., Vachon and Dobson,

1996, Wackerman *et al*., 1996, Fetterer *et al*.**,** 1998, Lehrer *et al.,* 1998, Vachon and Dobson, 2000). However, the detected wind direction has a 180° ambiguity, and it is not easy to remove the ambiguity. Meanwhile, the numerical meteorological model can acquire the wind direction with few missing values, and the accuracy of the wind direction is approximately 40 degrees (Takeyama *et al*., 2006).

1.4 Purpose of this dissertation

The purpose of this dissertation is to develop the method for the wind resource assessment. Firstly, sea surface wind speeds retrieved from SAR images using some GMFs are validated, and the most appropriate GMF is clarified in Japanese coastal waters. Secondly, the wind direction estimated by the numerical meteorological model is attempted to input as the GMF, and the effectiveness of the wind direction is examined. Finally, wind resource assessment is carried out by the means of these discussed methods.

1.5 Contexture

This dissertation consists of five parts. Chapter 1 is Introduction. In Chapter 2, some GMFs are attempted in Japanese coastal waters, and the most appropriate GMF is clarified. And then, in Chapter 3, an effectiveness of wind direction by numerical meteorological model, WRF as input to the GMF when the wind speed is retrieved from synthetic aperture radar images. In Chapter 4, the wind resource assessment is carried out using these discussed methods. Finally, general conclusions are described in Chapter 5.

References

Fetterer, F.; Gineris, D.; Wackerman, C. Validating a scatterometer wind algorithm for ERS-1 SAR. *IEEE Trans. Geosci. Remote Sens.*, **1998**, *36*, 479–492. DOI: 10.1109/36.662731.

Hasager, C. B.; Dellwik, E.; Nielsen, M.; Furevik, B. R. Validation of ERS-2 SAR offshore wind-speed maps in the North Sea, *Int. J. Remote Sens*. **2004**, *25*, 3817-3841.

Horstmann, J.; Lehner, S.; Koch, W.; Tonboe, R. Computation of wind vectors over the ocean using spaceborne Synthetic Aperture Radar. *Johns Hopkins APL Technical Digest*, **2000**; *21*, 1.

Hersbach, H.; Stoffelen, A.; Haan, S. An improved C-band scatterometer ocean geophysical model function: CMOD5. *J. Geophys. Res.* **2007**, *112*, 1-18.

Hersbach, H. Comparison of C-band scatterometer CMOD5.N equivalent neutral winds with ECMWF. *J. Atm. Oceanic Tech.* **2010**, *27*, 721–736.

Horstmann, J.; Koch, W.; Lehner, S.; Tonboe, R. Ocean Winds from RADARSAT-1 ScanSAR. *Canadian J. Remote Sens.* **2002**, *28*, 3, 524-533.

Lehner, S.; Horstmann, J; Koch, W.; Rosenthal W. Mesoscale wind measurements using recalibrated ERS SAR images. *J. Geophys. Res.* **1998**, *103*, C4, 7847-7856.

Monaldo, F.; Thompson, D.; Beal, R.; Pichel, W.; Clemente-Colón, P. Comparisons of SAR-derived wind speed with model predictions and ocean buoy measurements. *IEEE Transaction on Geoscience and Remote Sensing*, **2001**; *39*, 12: 2587-2600. DOI: 10.1109/36.974994.

Quilfen, Y.; Chapron, B.; Elfouhaily, T.; Katsaros, K.; Tournadre, J. Observation of tropical cyclones by high-resolution scatterometry. *J. Geophys. Res.* **1998**, *103*, C4, 7767-7786.

Shimada S.; Ohsawa T.; Chikaoka S.; Kozai K. Accuracy of the Wind Speed Profile in the Lower PBL as Simulated by the WRF Model, SOLA, **2011**, Vol. 7, 109−112, doi:10.2151/sola.2011-028

Stoffelen, A.; Anderson, D. Scatterometer data interpretation: Estimation and validation of the transfer function CMOD-4. *J. Geophys. Res.* **1997**, *102*, C2, 5767-5780.

Takeyama, Y.; Ohsawa T.; Kozai K. Estimation of coastal wind fields by synthetic aperture radar and mesoscale meteorological model, *RENEWABLE ENERGY 2006 Proceedings*, 10-12 Oct **2006**, Chiba, Japan, 845-848.

Vachon, P. W.; Dobson, F. W. Validation of wind vector retrieval from ERS-1 SAR images over the ocean. *The Global Atmosphere and Ocean System*. **1996**, *5*, 177-187.

Vachon, P. W.; Dobson, F. W. Wind retrieval from RADARSAT SAR images: selection of a suitable C-band HH polarization wind retrieval model. *Canadian Journal of Remote Sensing*, **2000**, *26*, 306-313.

Wackerman, C.; Rufenach, C.L.; Shuchman, R.A.; Johannessen, J.A.; Davidson, K.L. Wind vector retrieval using ERS-1 synthetic aperture radar imagery. *IEEE Trans. Geosci. Remote Sens.* **1996**, *34*, 1343-1352.

Chapter 2

Appropriate geophysical model functions for SAR wind speed retrieval

2.1 Introduction

Estimation of sea surface wind speed has been attempted since the 1980s using a microwave scatterometer and a geophysical model function (GMF), which describes the relationship between microwave backscatter, local incidence angle, relative wind direction and wind speed at 10 m height above the mean sea level (MSL). Nowadays, wind field maps using the GMF are practically utilized (e.g. APDRC surface wind fields from ASCAT and QuikSCAT; http://apdrc.soest.hawaii.edu/data/data.php).

Multiple GMFs with the common name CMOD (C-band model) have been developed. An early C-band GMF, CMOD2, was formulated as a prelaunch model for the ERS (European Remote Sensing Satellite) -1 based on airborne scatterometer data. CMOD4 (Stoffelen and Anderson, 1997) was developed based on both the ERS-1 scatterometer and Synthetic Aperture Radar (SAR) data. Although CMOD4 has been frequently validated in previous studies (Lehner *et al*.,1998, Horstmann *et al*.,2002, Hasager *et al*.,2004), Stoffelen (1998) suggested that CMOD4-retrieved wind speeds are negatively biased by 4%. In addition, CMOD4 cannot retrieve high wind speeds (24 m/s and above). Meanwhile, CMOD_IFR2 (Quilfen *et al*., 1998) was developed independently from CMOD4. CMOD_IFR2, and also calibrated for the ERS-1 scatterometer based on buoy and analysis data. CMOD5 was developed to overcome the weak points of CMOD4, and has been used recently (Hasager *et al*., 2011), but it still has negative biases (Hersbach *et al*., 2007). In order to eliminate this negative bias, the latest GMF, CMOD5.N (Hersbach *et al*., 2007, Hersbach, 2010), was developed by refitting 28 coefficients of CMOD5 to reduce the negative bias, and CMOD5.N retrieves 0.5 m/s higher wind speed than CMOD5 on average for the correction.

A distinguishing feature of CMOD5.N is that it can retrieve the equivalent neutral wind speed (ENW) (Liu *et al*.,1996), whereas CMOD4 and CMOD5 retrieve a non-neutral wind speed, which is referred to in this study as the stability-dependent

wind speed (SDW) meaning a real wind speed. A scatterometer and SAR do not directly measure the 10 m-height wind speed, but they observe microwave backscatter from the sea surface. The intensity of the backscatter depends on the sea surface roughness or frictional velocity, which can be related to the 10 m-height wind speed through the Monin-Obukhov similarity theory (Monin *et al.*, 1954). That is, in the surface layer, wind speed increases with height, and the deviation from the logarithmic profile is determined by atmospheric stability. Thus, ideally, the 10 m-height wind speed should be retrieved taking atmospheric stability into account, and this is possible using CMOD5.N. The CMOD5.N-retrieved ENW can be converted to a SDW taking the atmospheric stability into account by using external input data of sea surface temperature, air temperature and relative humidity. As an offset for atmospheric stability, a value of 0.2 m/s is added in CMOD5.N compared to CMOD5 (Hersbach, 2010) on average. Along with the 0.5 m/s enhancement applied to eliminate the negative bias mentioned above, the difference between the wind speeds retrieved by CMOD5.N and CMOD5 is 0.7 m/s on average. Meanwhile, CMOD_IFR2 also was adjusted to near neutral wind speeds (Quilfen *et al*., 1998).

The purpose of this study is to identify the most promising GMF for the SAR wind speed retrieval in Japanese coastal waters, which are greatly affected by complex coastal topography and variable atmospheric stability due to prevailing monsoon winds and warm and cold ocean currents. Four C-band GMFs; CMOD4, CMOD_IFR2, CMOD5 and CMOD5.N, are compared with each other using 106 ENVISAT (ENVIronmental SATellite) Advanced SAR images at two validation sites, Hiratsuka and Shirahama, in Japanese coastal waters. The methods are described in Section 2.2, accuracy of wind speed retrieval by four GMFs are shown in Subsection 2.3.1, and discussions on effect of short fetch, and the effectiveness of the correction for atmospheric stability with CMOD5.N are described in Subsections 2.3.2 and 2.3.3, respectively. Finally, conclusions are given in Section 2.4.

2.2 DATA and Methods

2.2.1 In-situ *measurements and synthetic aperture radar (SAR) images*

The two target coastal waters of this study are Hiratsuka and Shirahama in Japan, where there are offshore platforms conducting meteorological observations. The geographical locations of the Hiratsuka offshore platform (35° 18′ 20″ N, 139° 20′ 45″ E) operated by the Institute of Industrial Science (IIS) of the University of Tokyo, and the Shirahama offshore platform (33° 42′ 32″ N, 135° 19′ 58″ E) operated by the Disaster Prevention Research Institute (DPRI) of Kyoto University are shown in Figure 2.1. These platforms have distances of 1 and 2 km from coast lines, respectively. On the two platforms, 10-min-average wind speed and direction are measured at a height of 23 m above the MSL by a propeller anemometer. These measured wind speeds are used to validate the sea surface wind speeds retrieved from SAR images.

This study uses images from the C-band Advanced SAR onboard the ENVISAT satellite, launched by the European Space Agency in 2002. In total, 106 Advanced SAR images with HH polarization for a horizontal transmit and a horizontal receive, and VV polarization for a vertical transmit and a vertical receive (Hiratsuka: 33 images, and Shirahama: 73 images) recorded with 12.5 m pixel spacing for the Precision Image Product (IMP) and 75.0 m pixel spacing for Wide Swath Mode (WSM) are used to retrieve sea surface wind speeds. All 106 images are listed in Appendixes 2.1 (Hiratsuka) and 2.2 (Shirahama). The SAR images are smoothed to 400 m spatial resolution using the Cressman method (Cressman, 1959) to remove speckle noise. Though it is expected that these platforms themselves make errors in SAR images, these errors also can be eliminated by the smoothing as well as the speckle noise as previous study reported (Shankaranarayanan and Donelan, 2001).

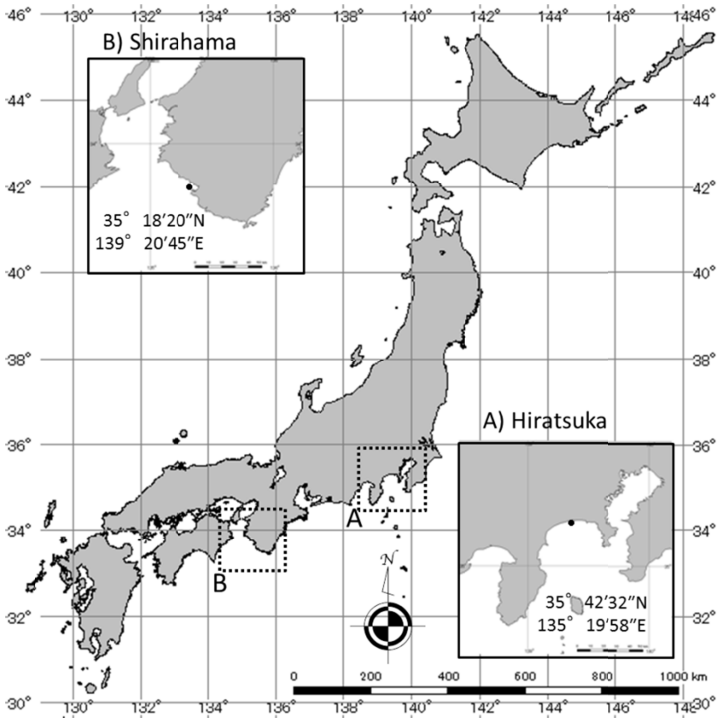

Figure 2.1 Geographical locations of the Hiratsuka (A) and Shirahama (B) offshore platforms (indicated by black circles in the inserts).

2.2.2 C-band geophysical model function (GMF)

Wind conditions retrieved from four C-band GMFs, CMOD4, CMOD5, CMOD_IFR2, and CMOD5.N are compared with *In-situ* measurements at Hiratsuka and Shirahama. The lower limit of wind speed retrieved from a GMF is known to be 1 to 3 m/s (Shankaranarayanan *et al*., 2001, Vachon and Dobson, 2000, ASCAT wind product user manual, 2012). Thus, this paper excludes *In-situ* wind speeds of less than 2 m/s at 23 m height from the validation. For CMOD4, the primary equation is written as

$$\sigma_{vv}^{0} = b_0\left(1.0 + b_1\cos\phi + b_3\tanh(b_2)\cos(2\phi)\right)^{1.6}, \tag{2.1}$$

for CMOD_IFR2, it is

$$\sigma_{vv}^{0} = 10.0^{\alpha+\beta\sqrt{v}}\left(1.0 + b_1\cos\phi + \tanh b_2\cos 2\phi\right) \tag{2.2}$$

and for CMOD5 and CMOD5.N, it is

$$\sigma_{vv}^{o} = b_0\left(1.0 + b_1\cos\phi + b_2\cos(2\phi)\right)^{1.6}, \quad (2.3),$$

where σ_{vv}^{0} is the VV-polarized Normalized Radar Cross Section (NRCS) and φ is the relative direction between the radar look direction and the wind direction. α, β and bi (i = 0, 1, 2, 3) are parameters, which depend on the radar incidence angle and wind speed. The relative wind direction should be acquired from other external sources, whereas the NRCS and the incidence angle can be obtained from an SAR image. *In-situ* wind directions are used as input to the GMFs in this study, although some methods to acquire wind directions from an SAR image itself or numerical simulations have been proposed (Vachon and Dobson, 1996, Wackerman *et al*., 1996, Takeyama et al., 2012).

Since all the C-band GMFs have been developed for VV-polarized NRCS (σ_{vv}^{0}), HH-polarized NRCS (σ_{hh}^{0}) must be converted by an empirical equation before the GMF processing. In order to convert from σ_{hh}^{0} to σ_{vv}^{0}, the equation (Mouche *et al*., 2005)

$$\frac{\sigma_{vv}^{0}}{\sigma_{hh}^{0}} = C_0(\theta) + C_1(\theta) + \cos\phi + C_2(\theta)\cos 2\phi \quad (2.4)$$

is applied. *Ci* (*i* = 0, 1, 2) are the ratios between HH and VV-polarized NRCSs for three wind directions, upwind, downwind and crosswind, respectively.

2.2.3 Height correction of in-situ *wind speed*

A GMF can retrieve the sea surface wind speed at a 10 m height above the MSL, whereas the *In-situ* wind speed is measured at 23 m above MSL at both offshore platforms. Thus, height correction of the *In-situ* wind speed is necessary to enable direct comparison with the retrieved wind speeds from the SAR images. For this height correction, the LKB code (Liu *et al.*, 1979) is used to estimate the 10 m-height wind speed from 23 m-height wind speed. The LKB code requires three kinds of input data, air temperature, relative humidity, and sea surface temperature (SST) for the estimation. This study principally uses values obtained from *In-situ* measurements. But, since air temperature is not measured at Hiratsuka, those simulated with the meteorological mesoscale model WRF (the Weather Research and Forecasting model, (http://wrf-model.org/index.php) are used instead of *In-situ* measurements. For this simulation, the Advanced Research WRF model version 3.0 is used, and the model configuration is shown in Appendix 2.1. In the LKB code, the following wind profile

based on the Monin-Obukhov similarity theory is used, taking the effect of atmospheric stability, expressed as Ψu(z/L), into account.

$$u = \frac{u_*}{\kappa}\left[ln\left(\frac{z}{z_0}\right) - \Psi_u\left(\frac{z}{L}\right)\right] \tag{2.5}$$

Here, u_* is frictional velocity, z_0 is roughness length, z is height, L is Monin-Obukhov length, and κ is the von Karman constant (=0.4). The relation between z_0 and u_* is given as

$$z_0 = 0.11\frac{\nu}{u_*} + z_{ch}\frac{u_*^2}{g} \tag{2.6}$$

where z_{ch} is Charnock's parameter with a value of 0.011 (Charnock, 1955), υ is the kinematic viscosity, and g is the acceleration due to gravity. The parameters of z_0 and u_* can be determined iteratively.

2.2.4 Conversion from ENW to SDW

ENW represents the wind at 10 m height for given surface stress in case the marine boundary layer is neutrally stratified, while SDW means real wind speed. In order to compare CMOD_IFR2- and CMOD5.N-retrieved ENW with *In-situ* wind speeds in the validation, the ENW is converted to SDW, which is comparable to the *In-situ* wind speed. Hereinafter, the SDW obtained from CMOD_IFR2 and CMOD5.N with the LKB code is referred to as CMOD_IFR2_SDW and CMOD5.N_SDW, while the ENW originally obtained from CMOD_IFR2 and CMOD5.N is referred to as CMOD_IFR2_ENW and CMOD5.N_ENW. The logarithmic wind profile,

$$u_{ENW} = \frac{u_*}{\kappa}\, ln\left(\frac{z}{z_0}\right) \tag{2.7}$$

is firstly used for the calculation of frictional velocity u_* from the ENW. Then the SDW is calculated using equation (2.5). The flowchart of the wind retrieval from an Advanced SAR image and its validation with an *In-situ* wind speed is depicted in Figure 2.2.

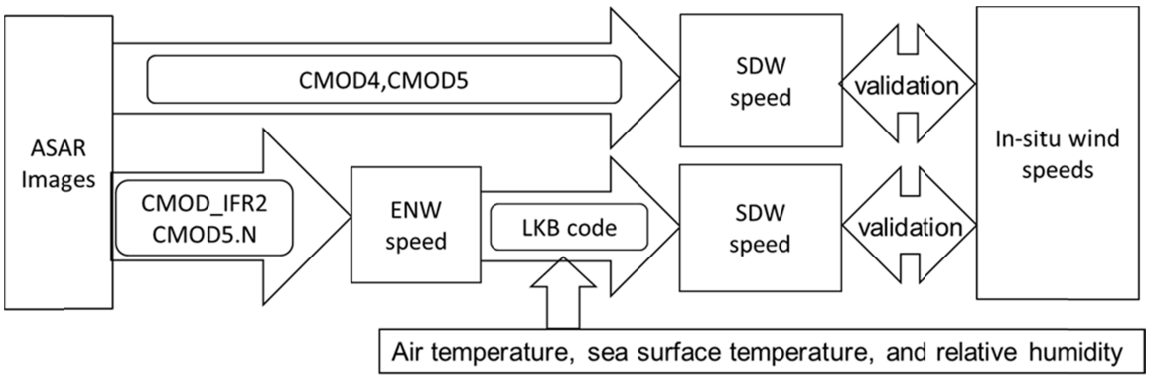

Figure 2.2 Flowchart of wind retrieval from an Advanced SAR image and validation with *In-situ* wind speed.

2.3 Results and Discussion

2.3.1 Accuracies of wind speed retrieval using four GMFs

Accuracies of the wind speed retrieved by four GMFs: CMOD4, CMOD_IFR2, CMOD5, and CMOD5.N, are compared at the two validation sites, Hiratsuka and Shirahama. Figure 2.3 shows relations between *In-situ* wind speeds and retrieved wind speeds from 33 SAR images using the four GMFs at Hiratsuka. The root mean square errors (RMSEs) of these SAR-retrieved wind speeds are 2.17 m/s (CMOD4), 2.34 m/s (CMOD_IFR2_SDW), 2.06 m/s (CMOD5) and 2.03 m/s (CMOD5.N_SDW), and the biases are –1.15 m/s (CMOD4), –1.31 m/s (CMOD_IFR2_SDW), –0.98 m/s (CMOD5) and –0.77 m/s (CMOD5.N_SDW), respectively. Thus, CMOD5.N_SDW has the smallest RMSE and bias at Hiratsuka. Figure 2.4 is the same as Figure 2.3, but for Shirahama, using 73 SAR images. The RMSEs of these SAR-retrieved wind speeds are 1.97 m/s (CMOD4), 2.05 m/s (CMOD_IFR2_SDW), 1.77 m/s (CMOD5) and 1.76 m/s (CMOD5.N_SDW), respectively and the biases are –1.10 m/s (CMOD4), –1.06 m/s (CMOD_IFR2_SDW), –0.64 m/s (CMOD5) and –0.42 m/s (CMOD5.N_SDW), respectively. All the statistic values are concluded in Table 2.1. These results show that CMOD5.N_SDW has the smallest RMSE and bias at Shirahama as well as Hiratsuka. Meanwhile, the retrieved wind speeds from WSM are also shown as squares in Figure

2.4, and the statistic values are shown in parentheses. No large difference is found in wind speed between WSM and IMP for all the GMFs.

All of the GMFs exhibit a negative bias in the retrieved wind speed at both validation sites. The absolute value of the negative bias in CMOD5.N_SDW is the smallest of all the GMFs, followed by CMOD5, CMOD4, and CMOD_IFR2_SDW in ascending order at both validation sites. These negative biases from CMOD4 and CMOD5 were reported in the previous study (Hersbach, 2010) as well. However, CMOD5.N, which has been developed to eliminate the negative bias, is found to still have a negative bias in this study. Moreover, the negative bias is much larger than that reported in previous studies such as (Abdalla and Hersbach, 2007, Portabella and Stoffelen, 2009), which showed that even the negative bias in CMOD5 is around –0.5 m/s. These facts indicate that the SAR wind speeds retrieved at Hiratsuka and Shirahama are affected by some factors that cause the larger negative biases. A possible factor for the negative bias is the effect of a short fetch as described in the previous study (Hersbach, 2010). This short fetch effect is discussed in detail in Subsection 2.3.2.

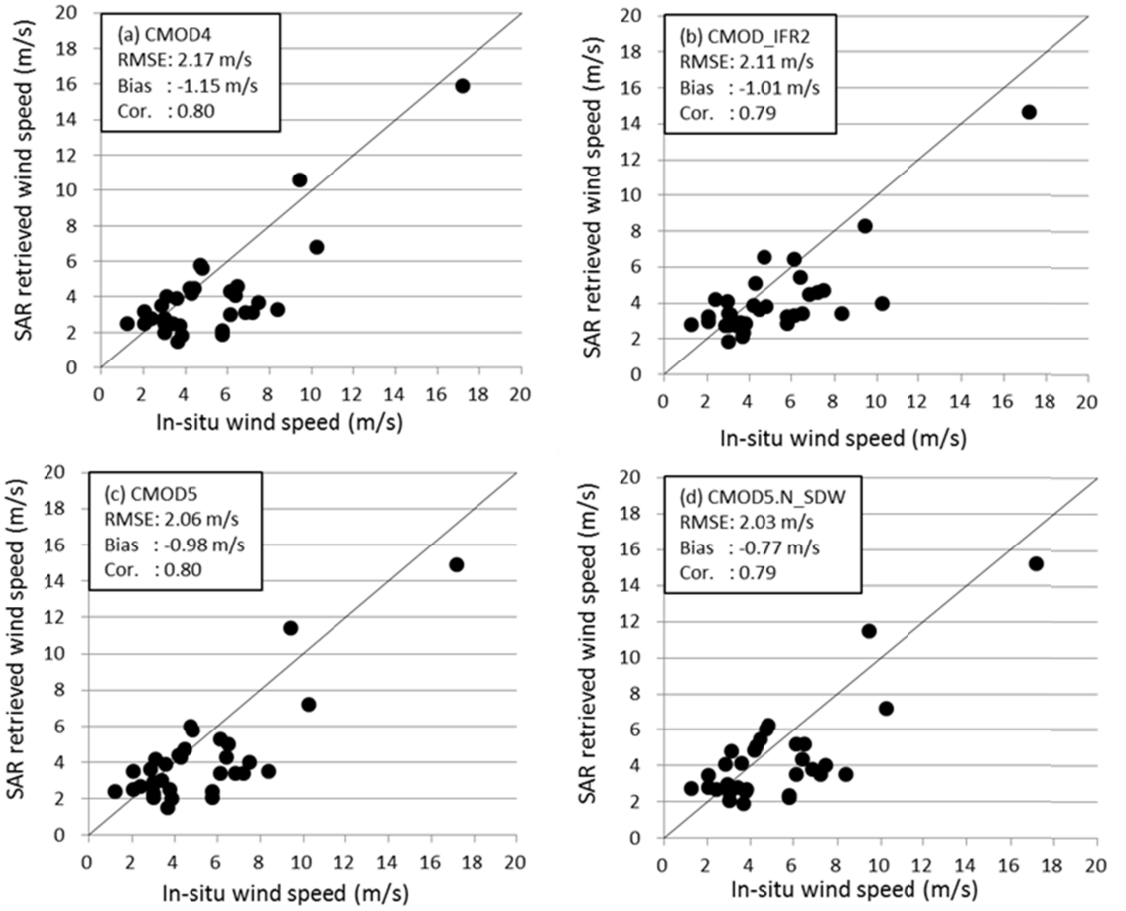

Figure 2.3 Relations between 33 SAR-retrieved wind speeds and *In-situ* wind speeds at Hiratsuka using four GMFs: (a) CMOD4, (b) CMOD_IFR2, (c) CMOD5, and (d) CMOD5.N.

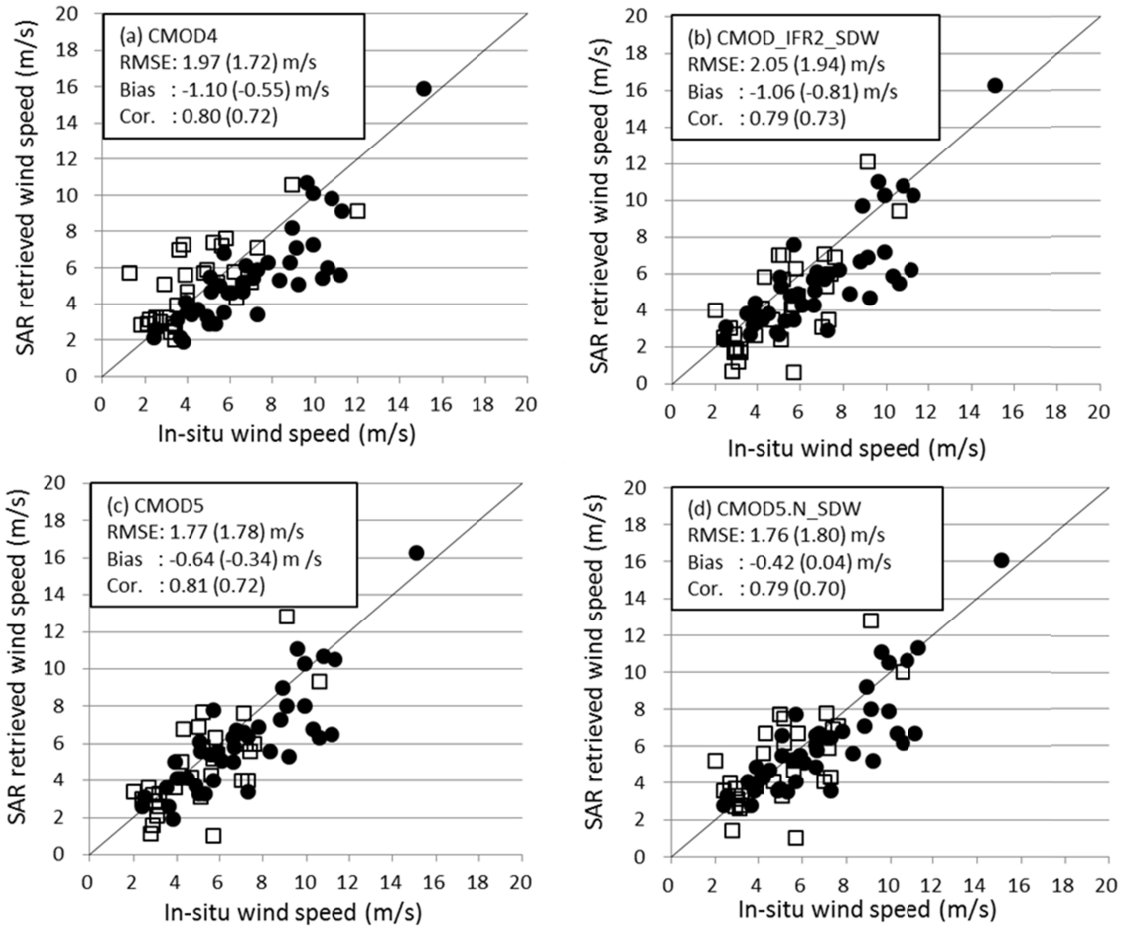

Figure 2.4 Same as Figure 2.3, but for 73 cases observed by IMP (daub circle) and WSM (square) at Shirahama. The statistics are for 73 cases, and those for WSM (31 cases) are in parentheses.

Table 2.1 RMSEs, biases and correlation coefficients of wind speeds retrieved by four GMFs at both Hiratsuka and Shirahama.

		CMOD4	**CMOD_IFR2_SDW**	**CMOD5**	**CMOD5.N_SDW**
Hiratsuka	RMSE (m/s)	2.17	2.34	2.06	2.03
	Bias (m/s)	−1.15	−1.31	−0.98	−0.77
	Correlation coef.	0.80	0.77	0.80	0.79
Shirahama	RMSE (m/s)	1.97	2.05	1.77	1.76
	Bias (m/s)	−1.10	−1.06	−0.64	−0.42
	Correlation coef.	0.80	0.79	0.81	0.79

2.3.2 Effect of short fetch on wind speed retrieval

In addition to wind speed, the fetch and duration of wind blowing over the sea surface can also change the sea surface roughness, especially in coastal waters. Thus, in this study, a short fetch is suspected to affect the sea surface roughness, resulting in the negative bias in the retrieved wind speed. To extract the short fetch effect on the SAR-retrieved wind speed, all the data are separated into two categories: offshore wind (blowing from land to sea) and onshore wind (blowing from sea to land). The onshore wind is defined as wind with a wind direction between 110 to 210 degrees at Hiratsuka, and 205 to 310 degrees at Shirahama, based on a threshold fetch of 30 km. This is because the previous study (Shimada *et al.*, 2004) shows that the wind speed growth with fetch is influenced by upwind terrain within 30 km from the coastline. Figure 2.5 shows scatter plots of 22 onshore winds at both validation sites for the four GMFs. The RMSEs of the SAR-retrieved wind speeds are all below 1.0 m/s: 0.74 m/s (CMOD4), 0.86 m/s (CMOD_IFR2_SDW), 0.64 m/s (CMOD5) and 0.88 m/s (CMOD5.N_SDW), and the biases are −0.12 m/s (CMOD4), –0.15 m/s (CMOD_IFR2_SDW), 0.20 m/s (CMOD5) and 0.57 m/s (CMOD5.N_SDW). All the negative biases shown in Figure 2.3 and 2.4 are obviously reduced in the case of only onshore wind.

Meanwhile, Figure 2.6 shows the same scatter plots as Figure 2.5 but for 84 offshore winds. The RMSEs are 2.16 m/s (CMOD4), 2.21 m/s (CMOD_IFR2_SDW), 2.22 m/s

(CMOD5) and 2.03 m/s (CMOD5.N_SDW), and the biases are –1.38 m/s (CMOD4), –1.40 m/s (CMOD_IFR2_SDW), –0.99 m/s (CMOD5) and –0.81 m/s (CMOD5.N_SDW), respectively. These statistic values are concluded in Table 2.2. All the RMSEs are greater than 2 m/s, and are obviously larger than those in Figures 2.3 and 2.4. In addition, the negative bias is larger compared to those in Figure 2.3 and 2.4. These results demonstrate that the negative biases, shown in Figures 2.3 and 2.4, are mainly due to the effect of the short fetch. In addition, it is found that only the wind speeds retrieved from WSM images have smaller negative biases, compared to those from both mode images. This tendency cannot be found in the onshore wind case (Figure 2.5). These results show that the wind speeds retrieved from the IMP image can be more easily affected by the short fetch.

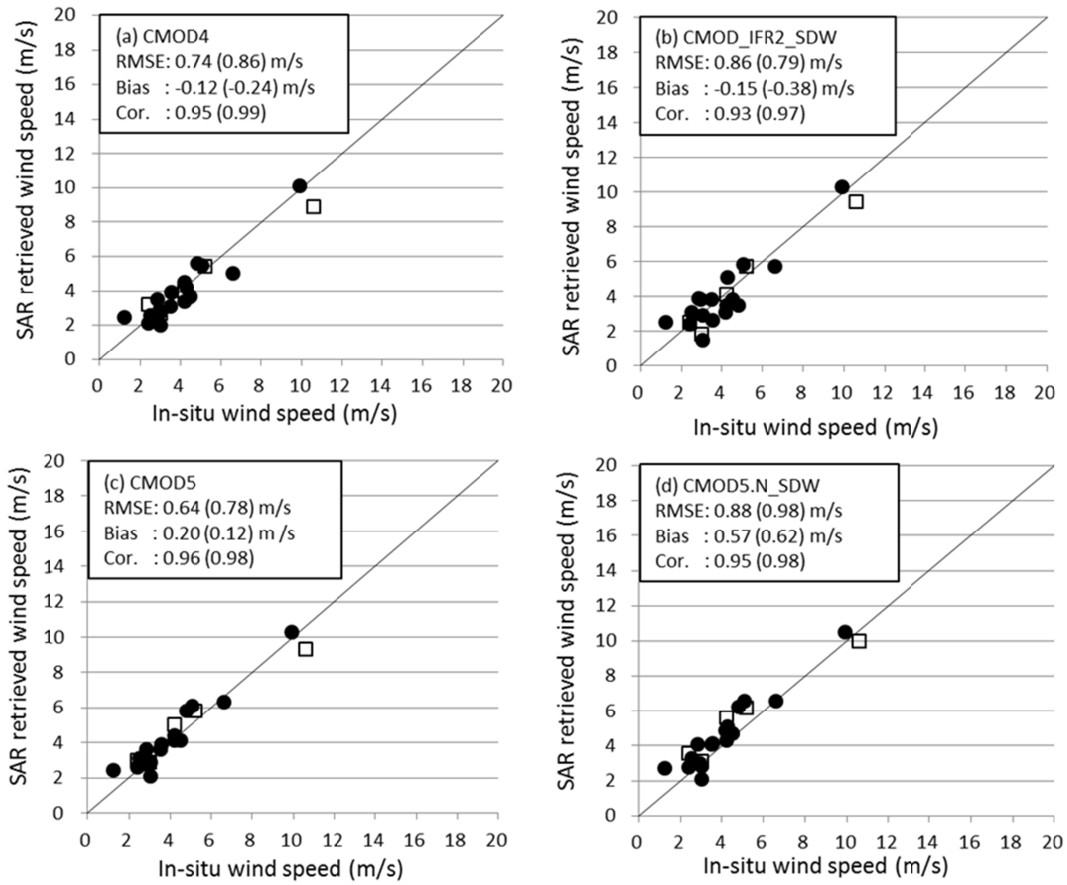

Figure 2.5 Same as Figure 2.3, but for 22 onshore winds by IMP (daub circle) and WSM (square) at both Hiratsuka and Shirahama. The statistics are for 22 cases, and those for WSM (5 cases) are in parentheses.

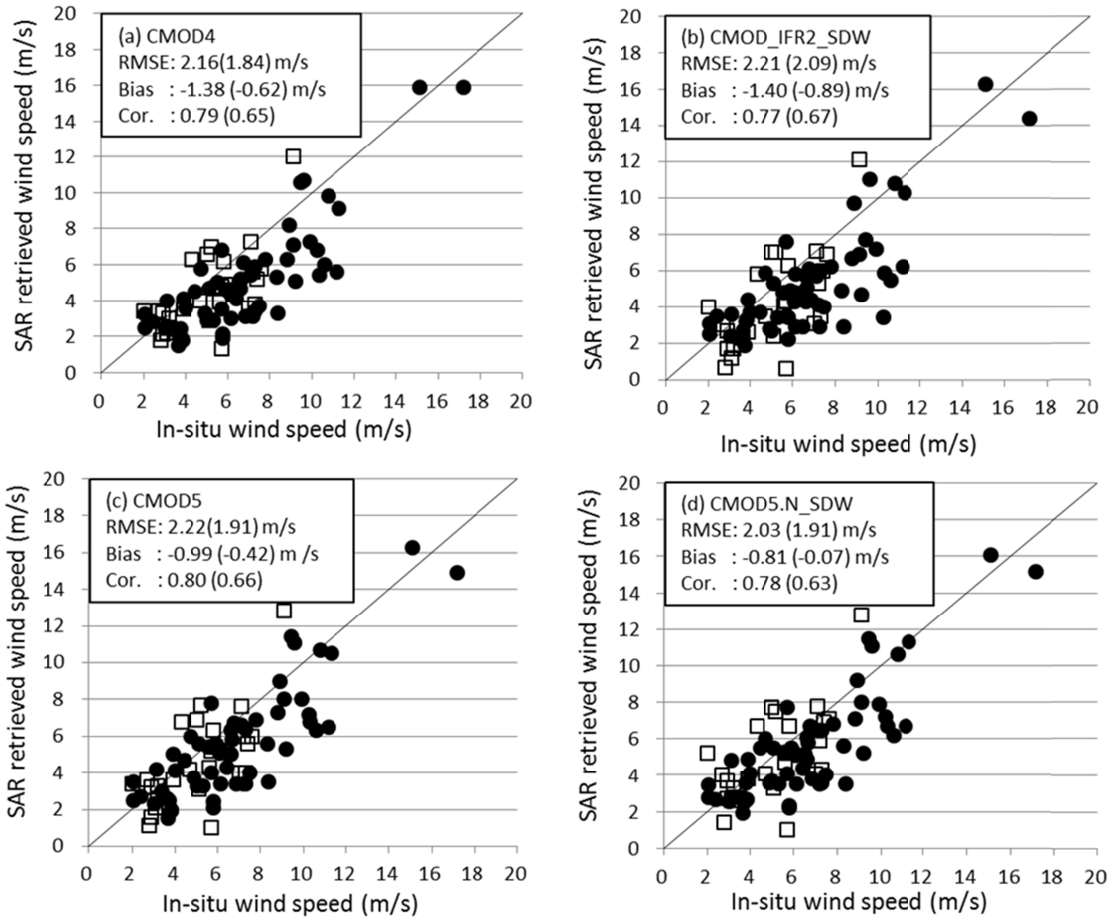

Figure 2.6 Same as Figure 2.3, but for 84 offshore winds by IMP (daub circle) and WSM (square) at both Hiratsuka and Shirahama. The statistics are for 84 cases, and those for WSM (26 cases) are in parentheses.

Table 2.2 RMSEs, biases and correlation coefficients of wind speeds retrieved by four GMFs at onshore and offshore winds.

		CMOD4	CMOD_IFR2_SDW	CMOD5	CMOD5.N_SDW
Onshore	RMSE (m/s)	0.74	0.86	0.64	0.88
	Bias (m/s)	−0.12	−0.15	0.20	0.57
	Correlation coef.	0.95	0.93	0.96	0.95
Offshore	RMSE (m/s)	2.16	2.21	2.22	2.03
	Bias (m/s)	−1.38	−1.40	−0.99	−0.81
	Correlation coef.	0.79	0.77	0.80	0.78

2.3.3 Effectiveness of atmospheric stability correction with CMOD5.N

In this subsection, effectiveness of the atmospheric stability correction is examined. Figure 2.7 shows monthly differences between SDW and ENW for *In-situ* measurements at Shirahama. Positive values indicate that SDW is larger than ENW. The differences between SDW and ENW range mostly between –0.9 and –0.2 m/s in the winter season (from October to March) when unstable conditions prevail, while the differences range from –0.5 to 1.2 m/s in the summer season (from April to September) when neutral and stable conditions tend to occur. Roughly speaking, the differences range from −1 to +1 m/s throughout the year. In Figure 2.8, monthly variation of the stability parameter z/L is shown. The parameters do not appear unless the CMOD5.N-retrieved wind speed is 2 m/s or higher because lower wind speeds give an extremely large value of the parameter. Figure 2.8 additionally shows that the stability parameter also indicates the seasonal variation of the atmospheric stability. In winter season, all values of z/L range from –7 to 0, while z/L ranges between –4 and 1 in summer season. From Figures 2.7 and 2.8, it is found that the difference between SDW and ENW shows seasonal variation, which depends on the actual atmospheric stability. This suggest that the atmospheric stability can cause an error of –1 to +1 m/s in the SAR retrieved wind speed when using

the GMFs that do not take into account the effect of atmospheric stability. Thus, the atmospheric stability correction is indispensable in the SAR wind speed retrieval in Japanese coastal water.

The relation between CMOD5, CMOD5.N_ENW and CMOD5.N_SDW is shown in Figure 2.9, based on the results in Subsection 2.3.1 and Figure 2.7. As shown in Figure 2.9, it is expected that the difference between CMOD5 and CMOD5.N_SDW decreases in the unstable condition, whereas it increases in the unstable condition. The small difference in the unstable condition is caused by the correction offset of about 0.7 m/s, which was enhanced when CMOD5.N had been developed from CMOD5 as shown in Figure 2.9.

In order to examine if CMOD5.N is effective for the atmospheric stability correction, the statistical values obtained from CMOD5.N_SDW and CMOD5 are shown in Table 2.3. In the neutral condition ($-1.0 < z/L \leq 0.1$), the RMSE with CMOD5.N_SDW (1.72 m/s) is slightly larger than CMOD5 (1.70 m/s). The differences of absolute biases are also few between CMOD5.N_SDW and CMOD5. Meanwhile, in unstable ($z/L \leq -1.0$) and stable condition ($0.1 < z/L$), CMOD5.N_SDW has a smaller RMSE than CMOD5. In particular, in the stable condition, the differences of RMSE and absolute biases between CMOD5.N_SDW and CMOD5.N are 0.15 m/s and 0.68 m/s, respectively, and the difference between CMOD5.N_SDW and CMOD5 is remarkable. These results indicate that atmospheric stability should be taken into account in the SAR wind speed retrieval in the seas with non-neutral conditions, and CMOD5.N is effective for the atmospheric stability correction.

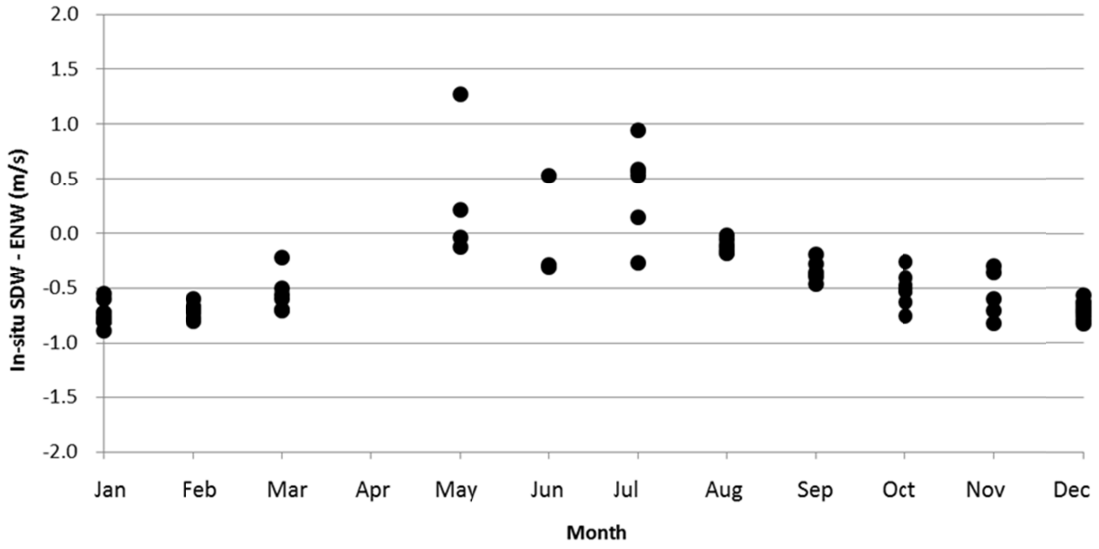

Figure 2.7 Monthly differences (m/s) between SDW and ENW for *In-situ* measurements at Shirahama.

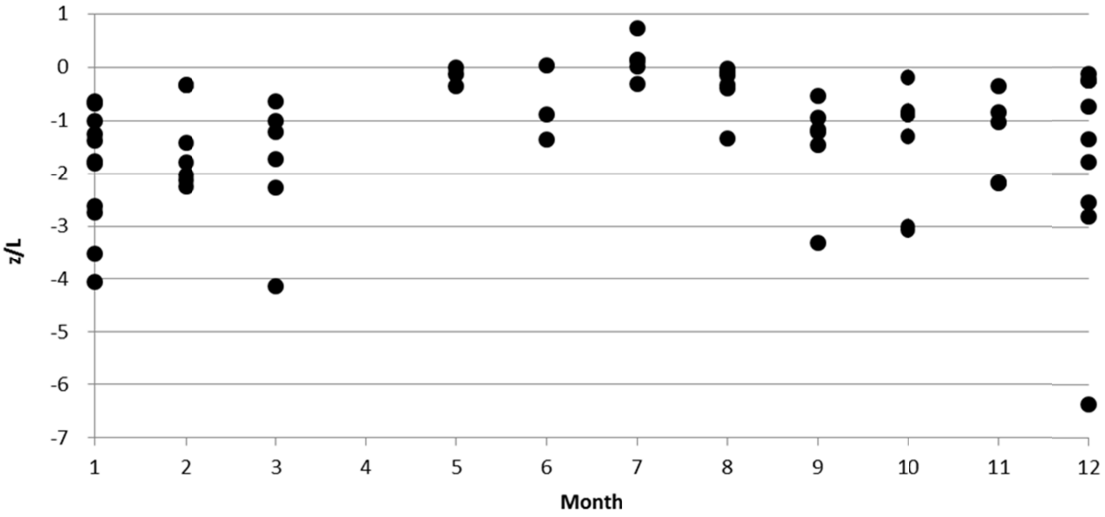

Figure 2.8 Monthly variation of z/L at Shirahama, but only 2 m/s or higher of the CMOD5.N-retrieved wind speed.

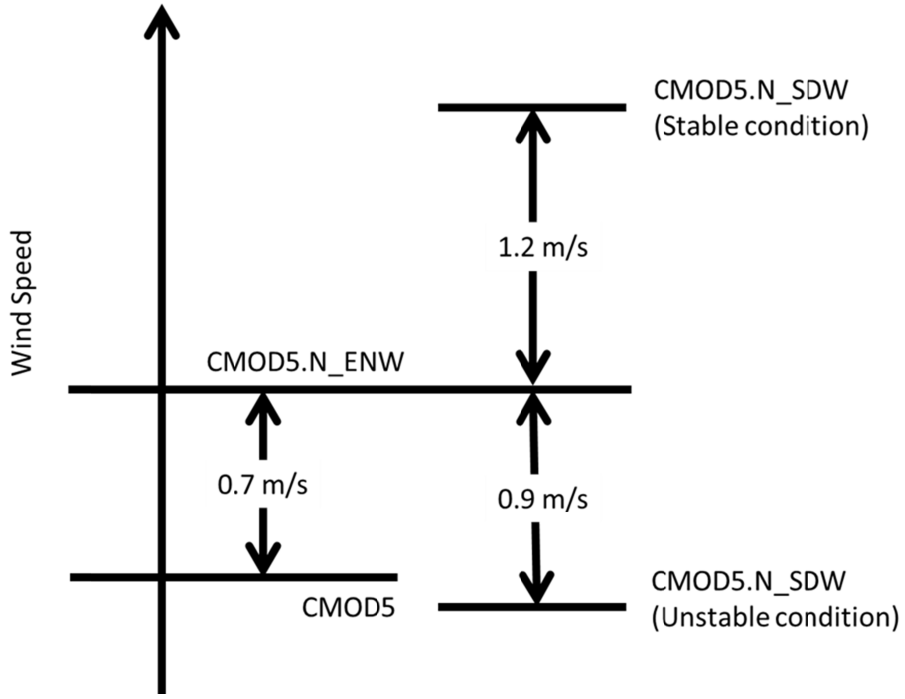

Figure 2.9 Relationship of retrieved wind speeds among CMOD5, CMOD5.N_ENW and CNOD5.N_SDW under stable and unstable atmospheric conditions.

Table 2.3 Comparison of statistics between CMOD5.N_SDW and CMOD5.

Atmospheric Condition		**Unstable (z/L ≤ −1.0)**	**Neutral (−1.0 < z/L ≤ 0.1)**	**Stable (0.1 < z/L)**
Bias (m/s)	CMOD5.N_SDW	−0.97	0.16	0.36
	CMOD5	−1.01	−0.11	-1.04
RMSE (m/s)	CMOD5.N_SDW	1.83	1.72	1.47
	CMOD5	1.85	1.70	1.62

2.4 Conclusion

In this section, four C-band geophysical model functions (GMFs) for sea surface wind speed retrieval: CMOD4, CMOD_IFR2, CMOD5, and CMOD5.N, are compared using 106 SAR images at two validation sites, Hiratsuka and Shirahama, in Japanese coastal waters. The effect of the correction of atmospheric stability, which is taken into account in the latest GMF CMOD5.N, is also examined since atmospheric stability is variable in Japanese coastal waters. The main results of this study are summarized as follows.

1) Of all the GMFs, the stability-dependent wind speed (SDW) retrieved with CMOD5.N and corrected for atmospheric stability with the LKB code (CMOD5.N_SDW) has the smallest root mean square error (RMSE) and the smallest bias at both Hiratsuka and Shirahama. The RMSEs are 2.03 m/s at Hiratsuka and 1.76 m/s at Shirahama, and the biases are −0.77 m/s at Hiratsuka and −0.42 m/s at Shirahama.

2) All of the GMFs exhibit a negative bias in the retrieved wind speed at both validation sites. By contrasting winds blowing onshore and offshore, only offshore winds were found to have a large negative bias. This indicates that the negative bias is primarily caused by short fetches from a coastline.

3) Atmospheric stability can cause an error of about –1 to +1 m/s in the SAR retrieved wind speed at Shirahama when using the GMFs that do not take the effect of atmospheric stability into account. CMOD5.N can reduce this error especially in non-neutral conditions, indicating that the use of CMOD5.N is effective for the atmospheric stability correction.

In short, at the moment, CMOD5.N is thought to be the most promising GMF for SAR wind speed retrieval in Japanese coastal waters. However, it is also clear that there is still ample room for future improvement. For instance, it is necessary to examine a larger number of wind speed samples because the samples used in this study were

mostly less than 12 m/s. Future work is also necessary for the investigation of the short fetch effect causing a large negative bias in winds blowing offshore.

References

Abdalla, S.; Hersbach, H. The technical support for global validation of ERS wind and wave Products at ECMWF. *ECMWF Contract Report to the European Space Agency*. **2007**, (http://www.ecmwf.int/publications/library/ecpublications/_pdf/esa/ESA_abdalla_hersbach.pdf).

ASCAT wind product user manual, **2012**, version 1.12, 27p.

Charnock, H. Wind stress on a water surface. *Quarterly Journal of the Royal Meteorological Society*. **1955**, *81*, 639-640.

Cressman, G. P. An operational objective analysis system. *Monthly Weather Review*. **1959**, *87*(10), 67-374.

Hasager, C. B.; Dellwik, E.; Nielsen, M.; Furevik, B. R. Validation of ERS-2 SAR offshore wind-speed maps in the North Sea, *Int. J. Remote Sen*. **2004**, *25*, 3817-3841.

Hasager, C. B.; Badger, M.; Peña, A.; Larsén, X.G.; Bingöl, F. SAR-Based Wind Resource Statistics in the Baltic Sea, *Remote Sens.* **2011**, *3*, 117-144, DOI: 10.3390/rs3010117.

Hersbach, H.; Stoffelen, A.; Haan, S. An improved C-band scatterometer ocean geophysical model function: CMOD5. *J. Geophys. Res.* **2007**, *112*, 1-18.

Hersbach, H. Comparison of C-band scatterometer CMOD5.N equivalent neutral winds with ECMWF. *J. Atm. Oceanic Tech.* **2010**, *27*, 721–736.

Horstmann, J.; Koch, W.; Lehner, S.; Tonboe, R. Ocean Winds from RADARSAT-1 ScanSAR. *Canadian J. Remote Sens.* **2002**, *28*, 3, 524-533.

Lehner, S.; Horstmann, J; Koch, W.; Rosenthal W., Mesoscale wind measurements using recalibrated ERS SAR images. *J. Geophys. Res.* **1998**, *103*, C4, 7847-7856.

Liu, W. T.; Katsaros, K.B.; Businger, J.A. Bulk parameterization of air-sea exchanges of heat and water vapor including the molecular constraints at the Interface. *J. Atmos. Sci.***1979**, *36*, 1722–1735.

Liu, W. T., Tang, W. Equivalent Neutral Wind. *JPL publication.* **1996**, *96-78*.

Monin, A. S.; Obukhov A. M. Basic regularity in tur- bulent mixing in the surface layer of the atmosphere, *Geofiz. Inst. Akad. Nauk SSSR*, **1954**, *24*, 163–187

Mouche, A. A.; Hauser, D.; Daloze, J.; Gueri, C. Dual-Polarization measurements at C-Band over the ocean: result from airborne radar observations and comparison with ENVISAT ASAR data. *IEEE Trans. Geosci. Remote Sens.* **2005**, *43*, 4, 753-769.

Portabella, M.; Stoffelen A. On scatterometer ocean stress. *J. Atmos. Oceanic Technol*., 2009, *26*, 368–382.

Quilfen, Y.; Chapron, B.; Elfouhaily, T.; Katsaros, K.; Tournadre, J. Observation of tropical cyclones by high-resolution scatterometry. *J. Geophys. Res.* **1998**, *103*, C4, 7767-7786.

Shankaranarayanan, K.; Donelan, M. A. A probabilistic approach to scatterometer model function verification. *J. Atmos. Sci.* **2001**, *106*, 19969-19990.

Shimada, T.; Kawamura H.; Shimada M.; Watabe I.; Iwasaki S. Evaluation of JERS-1 SAR images from a coastal wind retrieval point of view. *IEEE Trans. Geosci. Remote Sens*. **2004**, *42*, 3, 491-500.

Stoffelen, A.; Anderson, D. Scatterometer data interpretation: Estimation and validation of the transfer function CMOD-4. *J. Geophys. Res.* **1997**, *102*, C2, 5767-5780.

Stoffelen, A. Toward the true near-surface wind speed: error modeling and calibration using triple collocation. *J. Geophys. Res.* **1998**, *103*, 7755–7766.

Takeyama, Y.; Ohsawa, T.; Kozai, K.; Hasager, C. B.; Badger, M. Effectiveness of weather research and forecasting wind direction for retrieving coastal sea surface wind from synthetic aperture radar, *WIND ENERGY*, **2012**, Published online in Wiley Online Library.

Vachon, P. W.; Dobson, F. W. Validation of wind vector retrieval from ERS-1 SAR images over the ocean. *The Global Atmosphere and Ocean System*. **1996**, *5*, 177-187.

Vachon, P. W.; Dobson, F. W. Wind retrieval from radarsat sar images: Selection of a suitable C-band HH polarization wind retrieval model. *Can. J. Remote Sens.* **2000**, *26*, 4, 306–313.

Wackerman, C.; Rufenach, C. L.; Shuchman, R. A.; Johannessen, J.A.; Davidson, K.L. Wind vector retrieval using ERS-1 synthetic aperture radar imagery. *IEEE Trans. Geosci. Remote Sens.* **1996**, *34*, 1343-1352.

Appendix 2.1

List of 33 ENVISAT Advanced SAR images with corresponding *In-situ* measurements at Hiratsuka.

SAR				*In-situ*		WRF	
Date (year/month /day)	Time (hr: min: sec)	Polarization (HH or VV)	Observation mode	Wind direction (℃)	Wind speed (m/s) at 10 m	Sea temp. (℃)	Air temp. (℃)
2003/02/01	00:54:51	VV	IMP	3	6.1	17.8	8.6
2003/02/17	00:51:57	VV	IMP	350	3.7	18.1	11.6
2003/06/21	00:54:56	VV	IMP	213	3.8	23.8	25.3
2003/07/26	00:55:00	VV	IMP	5	5.8	24.3	25.5
2003/08/30	00:55:04	VV	IMP	19	3.6	26.5	28.0
2003/10/04	00:55:00	VV	IMP	38	3.4	26.0	21.0
2003/10/20	00:52:06	VV	IMP	1	8.4	24.2	18.5
2003/11/08	00:54:56	VV	IMP	117	3.0	24.4	20.9
2003/12/25	12:31:35	VV	IMP	233	17.2	20.2	15.7
2003/12/29	00:52:09	VV	IMP	259	9.4	20.1	13.4
2005/10/05	00:49:22	HH	IMP	40	3.0	22.6	22.0
2005/11/25	00:46:29	HH	IMP	24	4.7	22.9	14.8
2005/12/30	00:46:22	HH	IMP	18	2.4	16.9	7.2
2006/03/10	00:46:20	HH	IMP	357	10.2	17.1	10.2
2006/05/19	00:46:26	HH	IMP	17	4.4	20.5	21.5
2006/06/23	00:46:31	HH	IMP	298	2.0	22.6	22.4
2006/07/28	00:46:32	HH	IMP	168	4.3	24.4	25.4
2007/01/22	00:52:02	VV	IMP	352	7.5	18.7	9.7
2007/05/04	00:46:26	HH	IMP	121	3.6	21.6	20.2
2007/05/07	00:52:06	HH	IMP	174	3.0	21.1	19.8
2007/06/08	00:46:28	VV	IMP	146	4.2	21.7	21.2
2007/08/17	00:46:28	HH	IMP	146	2.8	29.4	30.7
2007/09/21	00:46:23	VV	IMP	183	1.2	25.9	25.7
2007/11/17	00:54:53	VV	IMP	3	5.8	22.8	13.7
2007/11/30	00:46:19	HH	IMP	353	6.4	20.2	13.3
2007/12/03	00:51:59	HH	IMP	212	7.2	19.6	15.3
2008/04/21	00:52:00	VV	IMP	8	6.9	19.3	19.7
2008/06/27	00:46:22	HH	IMP	83	3.1	21.0	22.2
2008/08/01	00:46:22	HH	IMP	165	2.9	22.2	20.9
2008/10/13	00:52:00	VV	IMP	113	4.8	27.6	27.1
2008/11/14	00:46:23	HH	IMP	23	6.1	24.6	21.5
2008/11/17	00:51:57	VV	IMP	354	6.5	21.4	17.5
2008/12/22	00:51:59	VV	IMP	91	2.0	22.6	17.9

Appendix 2.2

Same as Appendix 2.1, but for 73 images and *In-situ* measurements at Shirahama.

SAR				*In-situ*		WRF	
Date (year/month/day)	Time (hur:min:sec)	Polarization (HH or VV)	Observation mode	Wind direction (℃)	Wind speed (m/s) at 10 m	Sea Temp. (℃)	Air Temp. (℃)
2003/05/07	01:09:47	VV	IMP	114	3.6	21.4	22.3
2003/07/16	01:09:53	VV	IMP	296	6.6	25.2	24.5
2003/09/24	01:09:56	VV	IMP	59	11.2	26.4	24.9
2003/10/29	01:09:50	VV	IMP	347	10.3	24.0	18.5
2003/12/19	01:07:03	VV	IMP	347	15.1	21.0	12.0
2004/01/23	01:07:00	VV	IMP	322	7.8	18.9	6.4
2004/02/11	01:09:51	VV	IMP	320	3.9	19.7	10.1
2004/02/27	01:07:00	VV	IMP	308	9.9	20.7	9.5
2004/05/07	01:07:00	VV	IMP	268	4.5	23.2	21.8
2004/06/30	01:09:55	VV	IMP	64	5.3	25.2	25.7
2004/07/31	12:48:26	VV	IMP	115	11.3	27.7	27.7
2004/08/20	01:07:04	VV	IMP	259	5.1	27.5	27.4
2004/09/08	01:09:55	VV	IMP	286	2.5	27.5	27.4
2004/10/13	01:09:56	VV	IMP	20	8.9	24.5	23.1
2004/10/29	01:07:06	VV	IMP	93	5.7	22.0	21.4
2005/01/07	01:06:58	VV	IMP	10	7.3	18.4	12.6
2005/02/11	01:07:01	VV	IMP	331	6.1	17.1	8.3
2005/05/11	01:09:59	VV	IMP	247	3.5	20.0	18.8
2005/05/27	01:07:07	VV	IMP	176	3.8	21.7	21.1
2005/10/14	01:07:05	VV	IMP	96	5.0	26.4	25.5
2005/11/18	01:07:03	VV	IMP	6	6.8	23.4	14.5
2005/12/23	01:06:57	VV	IMP	326	9.6	19.9	8.9
2006/01/11	01:09:42	VV	IMP	358	5.9	19.2	9.5
2006/03/03	01:06:54	VV	IMP	317	9.1	18.3	8.3
2007/08/29	01:09:47	VV	IMP	244	2.4	30.3	29.3
2007/11/07	01:09:43	VV	IMP	16	4.0	24.6	19.8
2007/11/23	01:06:48	VV	IMP	352	9.9	23.3	13.3
2007/12/08	12:48:10	VV	IMP	176	5.7	22.2	15.4
2007/12/09	01:03:59	VV	IMP	340	8.3	21.7	12.8
2008/01/12	12:48:12	VV	IMP	348	8.8	20.2	11.1
2008/01/13	01:04:01	VV	IMP	347	9.2	20.8	10.3
2008/01/16	01:09:43	VV	IMP	349	7.1	20.7	11.6
2008/01/31	12:51:01	VV	IMP	7	6.6	20.9	10.2
2008/02/01	01:06:50	VV	IMP	355	5.5	20.2	9.2
2008/02/16	12:48:09	VV	IMP	323	10.8	18.9	9.0
2008/02/17	01:03:59	VV	IMP	342	10.6	19.6	8.2
2008/02/20	01:09:42	VV	IMP	345	6.6	19.5	10.0

2008/03/06	12:51:02	VV	IMP	72	4.9	18.9	13.5
2008/03/07	01:06:51	VV	IMP	337	6.7	18.4	11.4
2008/03/22	12:48:13	VV	IMP	244	4.2	18.0	15.7
2008/03/23	01:04:02	VV	IMP	159	7.3	18.0	17.4
2008/03/26	01:09:43	VV	IMP	354	5.1	18.5	14.6
	SAR				*In-situ*		
2010/06/25	01:01:06	VV	WSM	84	3.1	23.4	24.1
2010/07/11	01:01:03	VV	WSM	168	7.4	26.1	24
2010/07/27	01:01:00	VV	WSM	184	2	30.7	27
2010/07/30	01:01:06	VV	WSM	205	2.9	27.8	26.4
2010/08/12	00:00:57	VV	WSM	218	10.6	28.2	27.8
2010/08/15	01:01:03	VV	WSM	211	5.2	28.8	28.4
2010/08/18	01:01:09	VV	WSM	286	4.2	28.7	28.2
2010/08/31	01:01:00	VV	WSM	223	2.4	29.3	29
2010/09/03	01:01:06	VV	WSM	267	3	28.3	29.6
2011/10/30	01:01:07	VV	WSM	30	2.8	19.8	24.2
2011/12/07	01:01:14	VV	WSM	359	5.7	14.5	21.7
2011/12/10	01:01:04	VV	WSM	33	4.3	9.5	21.5
2011/12/18	01:01:11	VV	WSM	3	9.1	8.4	21.2
2010/06/27	12:12:56	VV	WSM	187	5	25.4	24
2010/07/13	12:12:53	VV	WSM	164	7.6	26.1	23.9
2010/08/14	12:12:47	VV	WSM	176	5.6	28	28.2
2010/09/05	12:12:56	VV	WSM	104	2.7	27.8	29.9
2010/09/18	12:12:47	VV	WSM	95	3.2	24	27.7
2010/09/21	12:12:53	VV	WSM	103	2.9	26.4	27.7
2011/10/18	12:12:58	VV	WSM	108	3.9	18.5	25.4
2011/10/26	13:13:04	VV	WSM	29	5.2	14.6	24.5
2011/10/29	12:12:54	VV	WSM	119	5.1	19.1	24.2
2011/11/06	13:13:01	VV	WSM	355	5.8	21.5	23.8
2011/11/25	13:13:04	VV	WSM	18	5.9	11	21.8
2011/12/06	13:13:01	VV	WSM	23	4.7	13.6	21.8
2011/12/17	12:12:58	VV	WSM	26	5.7	7.9	20.3
2011/12/28	12:12:55	VV	WSM	71	3.2	6.5	18.9
2012/01/06	01:01:15	VV	WSM	14	7.3	6.6	18
2012/01/09	01:01:05	VV	WSM	24	7.1	9.5	17.9
2012/01/05	13:13:01	VV	WSM	27	7.2	6.3	18.3
2012/01/16	12:12:58	VV	WSM	46	7	6.4	18.3

Appendix 2.3

The model configuration used in the WRF simulation.

Initial data		MANAL NGSST (0.05° × 0.05°, daily)		
Vertical resolution		28 levels (surface to 10 hPa)		
Nesting option		two-way nesting		
Domain		Domain 1	Domain 2	Domain 3
Horizontal		4.5 km	1.5 km	0.5 km
Grid points		100 × 100	100 × 100	100 × 100
Time step		27 sec	9 sec	3 sec
Physics option	Surface layer	Monin-Obukhov (Janjic Eta)		
	Planetary Boundary Layer	Mellor-Yamada-Janjic (Eta) TKE		
	Short wave radiation	Dudhia		
	Long wave radiation	RRTM		
	Cloud microphysics	WSM3		
	Cumulus parameterization	Kain-Fritsch (new Eta)	none	none
	Land surface	Five-layer soil		
4dda option		Enable including PBL	Enable excluding PBL	Enable excluding BL

MANAL: Japan Meteorological Agency Meso-Analysis

NGSST: New Generation Sea Surface Temperature

PBL: Planetary Boundary Layer

Chapter 3

Effectiveness of WRF wind direction for retrieving coastal sea surface wind from SAR

3.1 Introduction

A high accuracy representation of the wind is required for offshore wind resource assessment. Satellite observations appear to provide a reasonable method for estimation of the sea surface wind speed as an alternative data source (Hasager *et al.*, 2006, Beaucage *et al*., 2008, Badger *et al.,* 2010). The sea surface wind speed and direction have been observed by a satellite-borne wind scatterometer with a horizontal resolution on the order of several dozen kilometers. However, because of its coarse horizontal resolution, the scatterometer cannot give accurate wind measurements close to land. A satellite-borne synthetic aperture radar (SAR) with a higher horizontal resolution (e.g., 10 to 50 m) than the scatterometer has been used to retrieve the sea surface wind speed and direction in coastal waters. In previous studies, the SAR-retrieved wind speeds have been found to contain root mean square errors (RMSEs) of 2 to 3 m/s in coastal waters (e.g., Horstmann *et al.*, 2000, Monaldo *et al.*, 2001). These retrieved wind speeds from SAR images often have higher accuracies than those from a numerical meteorological model (e.g., Takeyama *et al.*, 2006**,** Kozai *et al.*, 2009). However, most validations have been performed in waters at least 10 km distant from the coastline. In the case of Japanese coastal waters with more complex onshore terrain and more unstable atmospheric conditions than the validation sites of these previous studies, sea surface wind speed retrieval from SAR images should be discussed in detail.

The primary effect of the sea surface wind speed is to change the surface roughness through centimeter scale waves, which are directly related to the intensity of microwave backscatter observed by SAR. The translation of the observed microwave backscatter to the wind speed requires an empirical geophysical model function (GMF) that describes the relationship among microwave backscatter, local incidence angle,

relative wind direction, and wind speed at 10 m above mean sea level (MSL). The relative wind direction is defined as the angle between the radar look direction and the wind direction. Estimation of the wind direction is thus indispensable for the wind speed retrieval from a SAR image using the GMF.

The following two methods are often used to estimate wind direction. The first method derives the wind direction from the SAR image itself using large-scale features that are aligned with local winds. The Fourier transform has often been used for the detection of the wind direction (e.g., Vachon and Dobson, 1996, Wackerman *et al*., 1996, Fetterer *et al*.**,** 1998, Lehrer *et al.,* 1998, Vachon and Dobson, 2000). Alternatively, a wavelet method (e.g., Du *et al.*, 2002), a local gradient method (e.g., Horstmann *et al.***,** 2002, Koch, 2004) and a projection model (e.g., Wacherman *et al.,* 2006) have also been used to derive the wind direction from the SAR image itself. However, these methods have three constraints. First, a kilometer-scale window size for the SAR image and uniform atmospheric conditiona are necessary because the typical wavelength of detected wind streaks is approximately 1 km (Gerling*,* 1986). The second constraint is that the wind streaks do not appear under low wind speed (< 8 m/s) conditions (Leher *et al.,* 1998). In the case of Japanese coastal waters, wind speeds are often under 8 m/s. Thus, the complete detection of wind direction in Japanese coastal waters using the method from all SAR images is difficult. The third constraint is that the detected wind direction has a 180° ambiguity. A method by which to determine the unique wind direction without external information on wind direction under any meteorological or topographical conditions has not been fully developed. The 180° ambiguity is actually eliminated by using *In-situ* or numerical model wind direction (Hasager *et al.,* 2004, Horstmann *et al.,* 2002). These constraints make adoption of the first method for Japanese coastal waters difficult because 1) the wind field is inhomogeneous due to complex terrain, 2) the wind speed is generally less than 8 m/s, and 3) there is little reliable information on wind direction to solve the 180° ambiguity. For these reasons, in the present study, we do not use the first method, which uses the wind direction derived from the SAR image itself.

The second method uses the wind direction obtained from external sources. Horstmann *et al.* (2000) used the wind direction obtained by the ERS-2 scatterometer measurements and showed that the retrieved wind speed had a RMSE of 2.7 m/s with

CMOD4. On the other hand, Monaldo *et al.* (2001) and Hasager *et al*. (2011) reported the estimation of wind speed with a RMSE of 1.76 m/s and 1.17 m/s, respectively, by using the wind directions from the navy operational global atmospheric prediction system (NOGAPS) model. These wind directions from external sources can supply the GMF with the data needed for wind speed retrieval. In particular, a mesoscale meteorological model is expected to provide more accurate wind directions for input to the GMF because the model can provide a two-dimensional wind direction field with good horizontal resolution, and temporally synchronized with the time when the SAR image was taken. However, few attempts have been made to date to use the wind direction from a mesoscale meteorological model in SAR wind retrieval (Beaucage *et al.*, 2007).

The present study examines the effectiveness of using the wind direction obtained from the weather research and forecasting model (WRF), which is a mesoscale meteorological model, as input to the GMF to retrieve an accurate sea surface wind field in coastal waters adjacent to complex onshore terrain. Using the WRF wind direction, wind speeds are retrieved from 42 ENVISAT ASAR images and compared with *In-situ* measurements at the Shirahama offshore platform in Tanabe Bay. In order to validate the effectiveness of this approach, the accuracies of the SAR-retrieved wind speed with the WRF wind direction are compared with those calculated using three other sources of wind directions: meso-analysis of the Japan Meteorological Agency (MANAL), the SeaWinds microwave scatterometer on QuikSCAT, and National Center for Environmental Prediction/National Center for Atmospheric Research final analysis using operational global analysis data (NCEP FNL).

3.2 DATA and Methods

3.2.1 In-situ *measurements and synthetic aperture radar images*

The target coastal area of the present study is Shirahama in Japan, where there is an offshore measurement platform (35°42′32″N, 135°19′58″E) (Figure 3.1), operated by the Disaster Prevention Research Institute (DPRI) of Kyoto University. The height of the platform is 23 m above MSL and its maximum diameter is roughly 10 m. Wind

speed and direction are measured using a propeller anemometer at the top of the platform, and the hourly 10-min-averaged values are archived in storage along with raw data measured at 10 Hz. These 10-min wind speeds at 23 m above MSL are corrected to wind speeds at 10 m above MSL using the LKB code (Liu *et al*., 1979) to allow direct comparison with the wind speed retrieved from SAR images. Here, it must be remembered that the *In-situ* wind speed is based on the 10-min-averaged value, whereas SAR observes the instantaneous condition of the sea surface.

The SAR images were all acquired by the C-band Advanced Synthetic Aperture Radar (ASAR) onboard the ENVISAT satellite, which was launched by the European Space Agency (ESA) in 2002. An example of a SAR image is shown in Figure 3.2. For the present study, 42 VV-polarized ASAR images were obtained in the precision mode for cases excluding those with extremely low wind speeds (< 2.0 m s^{-1}). Each processed image covers an area of approximately 100 × 100 km with a pixel size of 12.5 m. When the wind speed is retrieved, all SAR images are down-sampled by Cressman

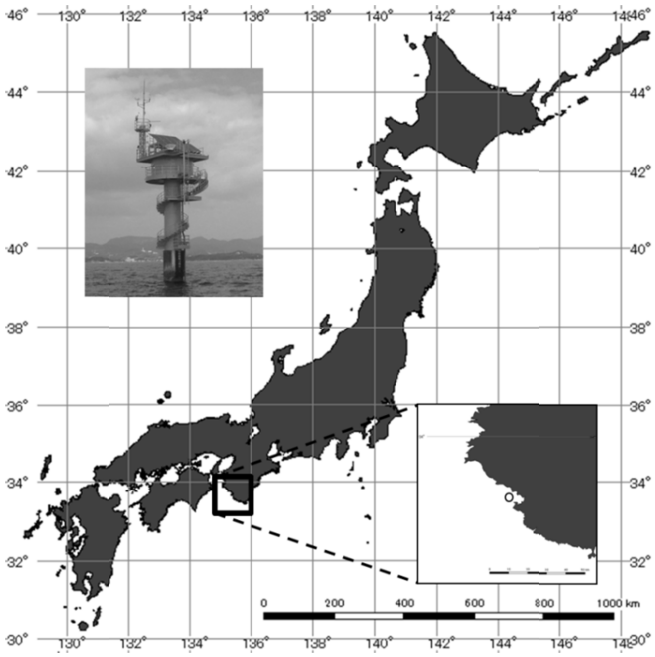

Figure 3.1 Geographical location and image of the Shirahama offshore platform (35°42′32″N, 135°19′58″E).

Figure 3.2 An example of a SAR image observed on May 26th, 2009, including the Shirahama offshore platform (white circle).

interpolation (Cressman, 1959). Generally, a pixel size of more than 400 to 500 m is used for SAR wind speed retrieval (Horstmann *et al*., 2000) because SAR images with a small pixel size are influenced by inherent noise. In the present study, the pixel size is resampled to 400 m with a 500 m diameter of influence for the interpolation.

In order to retrieve the sea surface wind speed, the latest GMF, CMOD5.N (Hersbach *et al*., 2010), is used. The primary equation of CMOD5.N is:

$$\sigma_{vv}^{o} = b_0\left(1.0 + b_1\cos\phi + b_2\cos(2\phi)\right)^{1.6} \tag{3.1}$$

where σ_{vv}^{0} is the VV-polarized Normalized Radar Cross Section (NRCS), which is strongly dependent on the small-scale roughness of the sea surface, which in turn is strongly dependent on wind speed. The symbol ϕ is relative wind direction, and the other parameters, b_0, b_1, and b_2, depend on radar incidence angle and wind speed.

CMOD5.N retrieves an Equivalent Neutral Wind (ENW) speed at 10 m height as proposed by Liu and Tang (1996), while stability dependent wind (SDW) speed is measured at the Shirahama offshore platform. Thus, the retrieved wind speed by CMOD5.N should be converted to SDW before comparison with *In-situ* measurements, and this is done using the LKB code in this study. Originally, the LKB code was used to

calculate ENW from measured wind speed, temperature, humidity and sea surface temperature (SST). For this conversion, the LKB code is used inversely. In the code, the logarithm wind profile

$$U_{ENW} = \frac{u_*}{\kappa} \ln\left(\frac{z}{z_0}\right) \tag{3.2}$$

is firstly used for the calculation of frictional velocity from ENW. Here, u_* is frictional velocity, z_0 is roughness length, and κ is the von Karman constant (= 0.4). Then, SDW is calculated using the following wind profile based on Monin-Obukhov similarity theory:

$$U_{SDW} = \frac{u_*}{\kappa}\left[\ \ln\left(\frac{z}{z_0}\right) - \psi_u(\zeta)\ \right] \tag{3.3}$$

considering atmospheric stability expressed as $\Psi_u(\zeta)$. In general, the ENW speed is higher than the SDW speed in unstable conditions, while it is lower in stable conditions. As input parameters, the temperature, humidity, and SST simulated with the Advanced Research WRF model version 3.0 are used in the inverse LKB code.

3.2.2 Wind directions used as input to CMOD5.N

In total, four sources of wind directions are examined as input to CMOD5.N in this study. One is from the WRF model and the others are from external data sources. The WRF model is a next-generation mesoscale numerical weather prediction system developed by seven institutes in the United States including NCEP and the National Center for Atmospheric Researches (NCAR). In this study, the WRF model calculates wind direction with a 500 m horizontal resolution and 28 vertical layers. MANAL and the New Generation Sea Surface Temperature (NGSST), which are 6-hourly 10 × 10 km mesoscale analysis provided from Japan Meteorological Agency (JMA) and daily 0.05 × 0.05° sea surface temperature provided from Tohoku University, respectively, are used as initial and lateral boundary conditions for the WRF model. The WRF is set up with three domains with horizontal resolutions of 4.5 km, 1.5 km and 500 m, respectively, gradually focusing on the Shirahama site. The detailed configuration of the WRF simulation is indicated in Table 3.1. It is same as Appendix 2.3. The simulated WRF

wind direction is provided as an input to CMOD5.N in order to retrieve wind speed from SAR images, and then the retrieved wind speed is validated against the *In-situ* measured wind speed. Additionally, simulated temperature, humidity, and SST by WRF are used for the conversion from ENW to SDW through the use of the LKB code as described in the previous section.

For comparison, three sources of external wind direction estimates, from MANAL, QuickSCAT (http://podaac-www.jpl.nasa.gov/dataset/QSCAT_LEVEL_2B_COMP_12) and NCEP FNL (http://dss.ucar.edu/datasets/ds083.2/) are also used as input to CMOD5.N. The temporal resolution (TR) and horizontal resolution (HR) of each wind direction source are summarized in Table 3.2. Both the HR and TR of the MANAL wind direction are the smallest of the three external wind directions, and are 6-hourly (or 3-hourly after Feb. 28th, 2009) and 10 × 10 km, respectively. As for QuikSCAT, the level 2B ocean vector wind product, provided by National Aeronautics and Space Administration/Jet Propulsion Laboratory, is used. The product has a 12.5 × 12.5 km HR, and the TR is once or twice a day, which is the largest of the three. The NCEP FNL wind direction has the largest HR of 1.0 × 1.0° of all the wind directions and the TR is 6 hours. The wind direction at the validation site is defined as the value at the nearest grid point and time of each external data source.

Table 3.1 Model configuration for the WRF simulation used in this study.

Initial data		MANAL NGSST (0.05°x 0.05°, daily)		
Vertical resolution		28 levels (surface to 10 hPa)		
Nesting option		two-way nesting		
Domain		Domain 1	Domain 2	Domain 3
Horizaontal		4.5 km	1.5 km	0.5 km
Grid points		100 x 100	100 x 100	100 x 100
Time step		27 sec	9 sec	3 sec
Physics option	Surface layer	Monin-Obukhov (Janjic Eta)		
	Planetary Boundary Layer	MYJ (Eta) TKE		
	Short wave radiation	Dudhia		
	Long wave radiation	RRTM		
	Cloud micropysics	WSM3		
	Cumulus parameterization	Kain-Fritsch (new Eta)	none	none
	Land surface	Five-layer soil		
4dda option		Enable including PBL	Enable excluding PBL	Enable excluding PBL

Table 3.2 Temporal and horizontal resolutions of five sources of wind direction data used in this study.

Wind direction	Temporal resolution	Horizontal resolution
In-situ	1 hour	on site
WRF	1 hour	500 × 500 m
MANAL	6 hours (00, 06, 12, 18 UTC) or 3 hours (00, 03, 06, 09, 12, 15, 18, 21)	10 × 10 km
QuikSCAT	1 day or 12 hours	12.5 × 12.5 km
NCEP	6 hours (00, 06, 12, 18 UTC)	1.0 × 1.0 °

3.3 Results and discussion

3.3.1 Accuracy of SAR retrieved wind speed with WRF wind direction

As the first step toward the validation, the *In-situ* measured wind direction is used as input to CMOD5.N in order to obtain reference values for the accuracy of the SAR-retrieved wind speed. Figure 3.3a indicates the accuracy of the SAR-retrieved wind speed using the *In-situ* wind direction in comparison with *In-situ* measured wind speed at the Shirahama offshore platform. The bias and RMSE for the 42 retrieved wind speeds are -0.75 m/s and 1.71 m/s, respectively. The bias and RMSE are defined as

$$Bias = \frac{1}{N}\sum_{i=1}^{N}\left(x_i - y_i\right) \tag{3.4}$$

and,

$$RMSE = \sqrt{\frac{1}{N}\sum_{i=1}^{N}\left(x_i - y_i\right)^2} \tag{3.5}$$

where, x is the SAR retrieved wind speed, y is the *In-situ* wind speed and N is the number of samples. The SAR wind speed retrieved without any information on wind direction is calculated as another extreme reference value, by taking the average of the

wind speeds for the entire range of wind directions from 0° to 359° in CMOD5.N. Figure 3.3b shows the accuracy for the case without information on wind direction (No info), and the bias and RMSE are -0.48 m/s and 2.24 m/s, respectively. This result indicates that the wind speed can be retrieved with a RMSE of at most 2.24 m/s, even if no information on wind direction is available. In the case of using the WRF wind direction (Figure 3.3c), the bias and RMSE are -1.31 m/s and 2.15 m/s, respectively. The RMSE is larger than that using the *In-situ* wind direction by 0.44 m/s, which corresponds to 6.3 % of the mean *In-situ* wind speed (7.0 m/s). It seems reasonable that the RMSE (2.15 m/s) lies between the two reference values (1.71 and 2.24 m/s), although the bias is more negative than the two reference cases.

Table 3.3 shows the bias and RMSE values shown in Figure 3.3 together with those obtained using wind directions from three external sources: MANAL, QuikSCAT and NCEP FNL. Focusing on the Mean Absolute Error (MAE) in wind direction, which is defined as

$$MAE = \frac{1}{N}\sum_{i=1}^{N}\left|x_i - y_i\right| \tag{3.6},$$

the WRF wind direction is found to have the lowest MAE (35.4°), followed by MANAL (42.9°), QuikSCAT (58.5°), and NCEP FNL (79.4°). On the other hand, the RMSE in the retrieved wind speed ranges between 1.96 and 2.81 m/s. While the NCEP FNL wind direction, which has the worst MAE, exhibits the highest RMSE, the lowest RMSE is achieved using the QuikSCAT wind direction, which is the second-worst wind direction. In other words, the use of the most accurate wind direction (i.e., the WRF wind direction) does not yield to the most accurate wind speed retrieval. Apparently, the effectiveness of using accurate WRF wind direction as input to the GMF cannot be confirmed based only on Table 3.3.

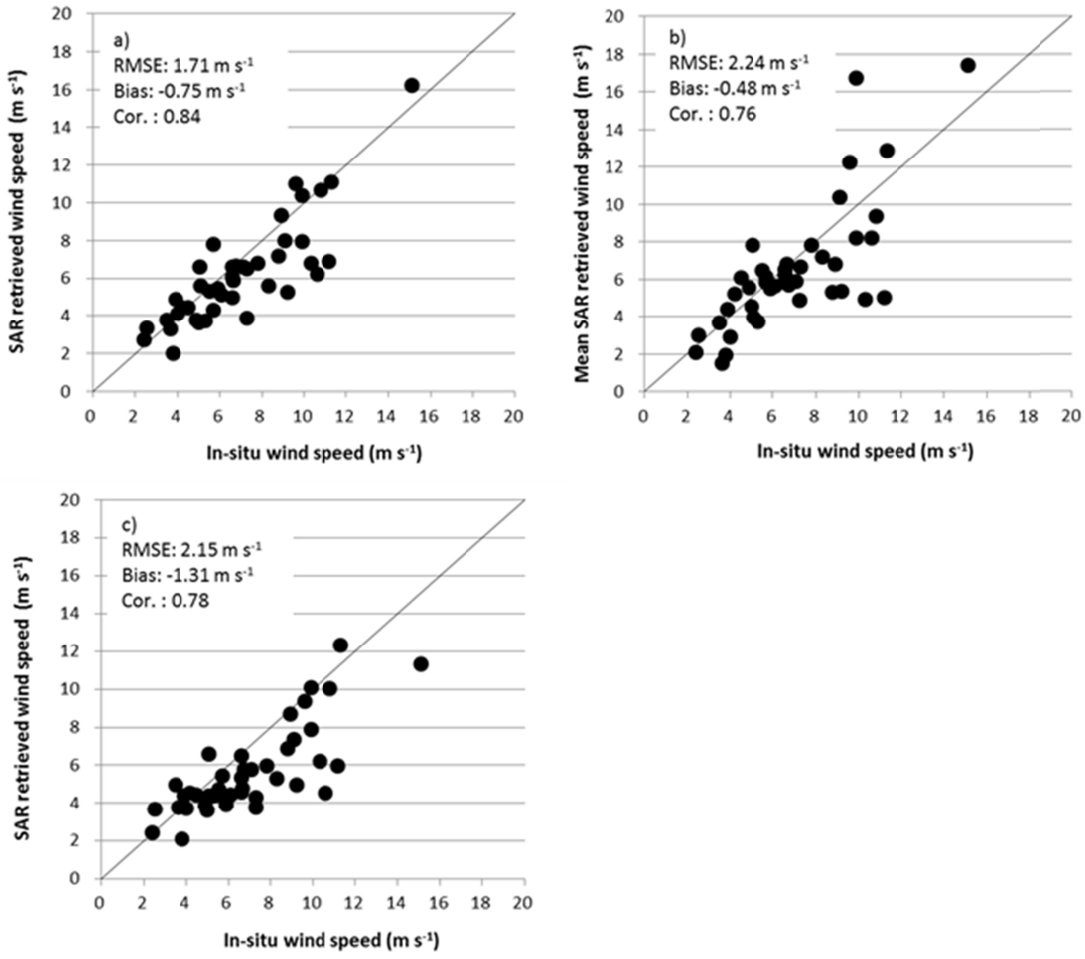

Figure 3.3 Accuracies of the SAR wind speeds retrieved by CMOD5.N (a) with *In-situ* wind direction, (b) without information on wind direction, and (c) with the WRF wind direction, against *In-situ* wind speed at the Shirahama offshore platform.

Table 3.3 Mean absolute error (MAE) in wind direction and bias and RMSE in retrieved wind speed for each source of wind direction data.

Wind direction	In-situ	No Info.	WRF	MANAL	QuikSCAT	NCEP FNL
MAE (degrees)	-	-	35.4	42.9	58.5	79.4
Bias (m s^{-1})	-0.75	-0.48	-1.31	-0.43	-0.73	-0.17
RMSE (m s^{-1})	1.71	2.24	2.15	2.11	1.96	2.81

3.3.2 Relationships between input wind direction and output wind speed

The reasons why the input of a more accurate wind direction does not lead to the retrieval of a more accurate wind speed in CMOD5.N are discussed here. Firstly, in Figure 3.3, the differences among the three retrieved wind speeds become more noticeable at higher wind speed, rather than at lower wind speeds. To show this result more clearly, Figure 3.4 illustrates the error in the retrieved wind speed with respect to the *In-situ* measured wind speed, and shows that, in all cases, the error becomes larger at higher wind speeds. This is partly due to the sensitivity of CMOD5.N to wind speed and direction, and is as explained in Figure 3.5. This figure shows the wind speeds that CMOD5.N is supposed to output as a function of relative wind direction for several values of NRCS at a constant incidence angle. It is found that while only slight changes of wind speed with relative wind direction can be seen at lower NRCS values (lower wind speeds), the directional change rapidly becomes greater as the NRCS value (wind speed) increases. In other words, as the wind speed increases, the SAR-retrieved wind speed can be more easily affected by uncertainty of wind direction. Conversely, if the wind speed is sufficiently low enough, the accuracy of the SAR-retrieved wind speed is not greatly changed regardless of the wind direction used as input to CMOD5.N. The mean wind speed of 7.0 m/s at the Shirahama offshore platform is probably not high enough to be greatly affected by the accuracy of the input wind direction, which is one of the main reasons why the WRF wind direction does not achieve the best retrieval of wind speed.

To identify additional reasons, the RMSE in the case of using *In-situ* wind direction is compared with the case of using no information on wind direction. As shown in Figure 3.3, even use of the *In-situ* wind direction exhibits a RMSE of 1.71 m/s, whereas the RMSE increases to 2.24 m/s in the case without information on wind direction. The difference between these cases is 0.53 m/s, which equals 31% of the RMSE of the *In-situ* wind direction case. This implies that the error caused by the uncertainty of wind direction corresponds to approximately 30% of the total error. Thus, it is thus plausible that errors from factors other than wind direction are sufficiently

large enough that the effectiveness of using better wind direction information is difficult to detect.

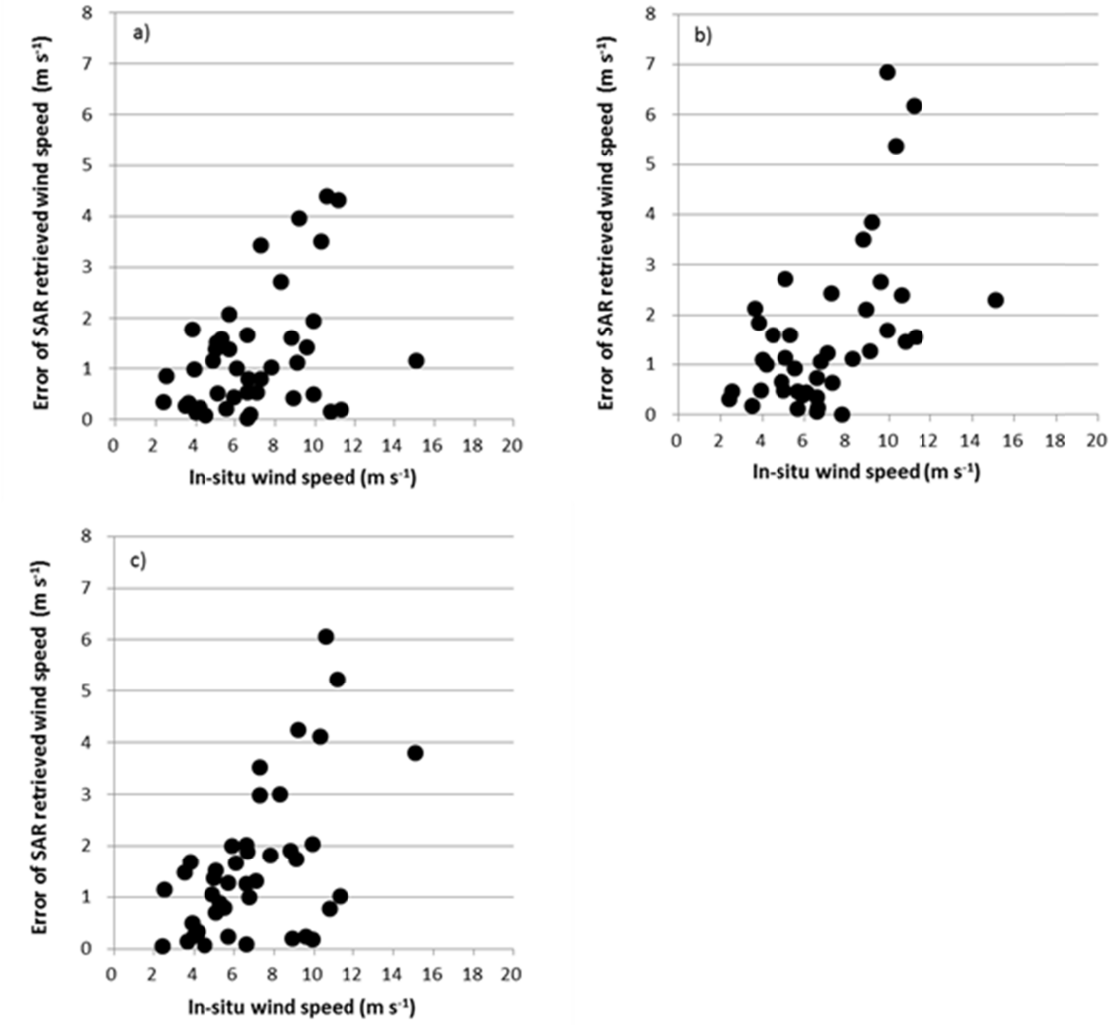

Figure 3.4 Dependency of the errors of SAR-retrieved wind speeds on wind speed using: (a) *In-situ* wind direction, (b) without information on wind direction and c) the WRF wind direction.

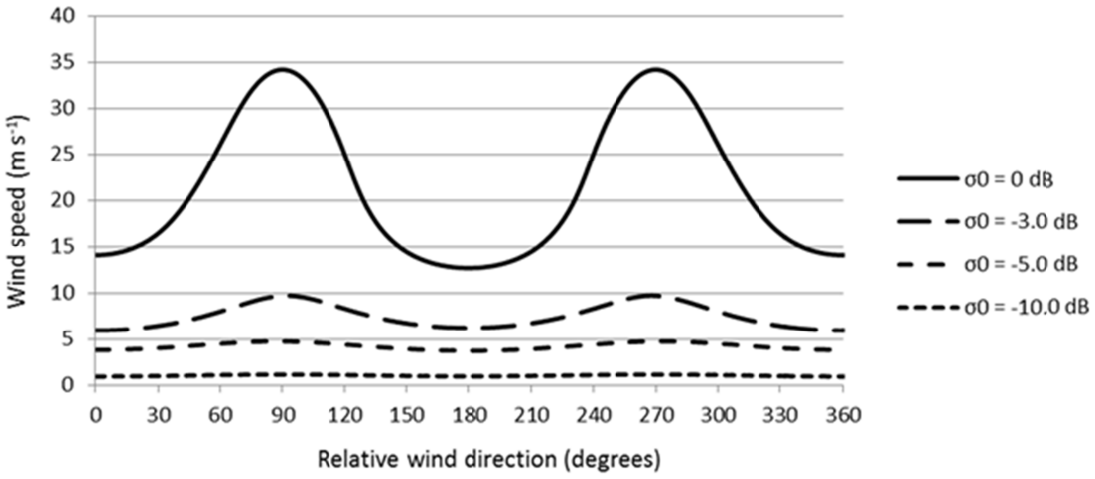

Figure 3.5 Dependency of the SAR-retrieved wind speed on relative wind direction and NRCS (σ^0) in CMOD5.N for the incidence angle of 20.0 degree.

3.3.3 Error factors other than wind direction

For SAR wind speed retrieval in coastal waters, it is important to confirm whether the wind speed is affected by geographical factors such as fetch, shallow water depth, coastlines, and land on the windward side, etc. Shimada *et al.* (2004), who had investigated the accuracy of wind speeds retrieved from the L-band SAR on JERS-1, indicated that the distance from the coastline influences the growth of wind speed and that offshore winds (blowing from land to sea) tend to have a negative bias. Moreover, Hersbash *et al.* (2010) also suggested that in coastal waters with offshore winds, a lack of consideration for the enhanced Charnock parameter, which is a parameter connecting surface roughness and frictional velocity, leads to negative biases at lower wind speeds.

Thus, in this section, the accuracies of SAR wind speeds are examined again with the four sources of wind directions from WRF, MANAL, QuikSCAT and NCEP FNL only for cases of onshore winds (blowing from sea to land), which are thought to be mostly free from terrain effects. The onshore wind is defined at the study site as wind blowing from 180° to 310°, corresponding to directions with a fetch of more than 20 km. Only 10 SAR images are classified as having an onshore wind, whereas the other 32 images are cases of offshore wind. Statistic values of the SAR wind speed retrieved with the *In-situ* wind direction are confirmed in each case of onshore and offshore wind

before the analysis. The RMSEs in the SAR wind speed are respectively 1.91 m/s (offshore) and 0.75 m/s, (onshore), and the biases are -1.10 m/s (offshore) and 0.35 m/s, (onshore). There are obviously error factors associated with terrain effects for the SAR wind speed retrieval in coastal areas. The results of the analysis with the four sources of wind directions are shown in Figure 3.6. First, the biases in wind speed shown in Figure 3.6 become larger than those in Table 3.3, and are mostly positive, indicating that the negative bias caused by terrain is removed by considering onshore winds. The RMSEs are much lower than for the results including both onshore and offshore winds. For onshore winds the RMSE is 0.96 m/s in the case of using the WRF wind direction, and this value is much lower than the values from MANAL, QuikSCAT and NCEP FNL wind directions. The difference between this RMSE and that with the *In-situ* wind direction (0.75 m/s) is 0.21 m/s (only 3% of mean wind speed), which is comparable to those validated in open oceans in previous studies (e.g., Horstmann *et al.*, 2000, Monaldo *et al.*, 2001). This RMSE is also lower than that for WRF wind speed (1.12 m/s) (see Figure 3.6f). On the other hand, NCEP FNL, which has the highest MAE in wind direction, has the highest RMSE of 2.00 m/s, and the value is approximately three times higher than the RMSE from the *In-situ* wind direction. In conclusion, when limited to onshore winds, which have few factors other than wind direction (e.g., fetch, shallow water depth, coastline, land on the wind ward side etc.), the input of the most accurate wind direction (WRF) leads to the output of the most accurate wind speed, while the least accurate wind direction (NCEP FNL) yields the least accurate wind speed.

The MANAL wind direction leads to less accurate wind speeds than the QuikSCAT wind direction, though the MAE of the MANAL wind direction is lower than that of the QuikSCAT wind direction. This uncorrelated order appears to occur because of the nonlinearity of CMOD5.N. As an example of its nonlinear nature, Figure 3.7 shows the differences in the CMOD5.N-retrieved wind speeds between a given wind direction and a given wind direction plus the MAE of the external wind directions with constant values of NRCS and incidence angle. The differences are shown as

$$\Delta U = U(\phi + MAE) - U(\phi) \tag{3.7}.$$

The NRCS and incidence angle are assumed to be -4.0 dB and 20.0 °, respectively. Note that the differences are calculated without NRCSs from SAR images. In Figure 3.7, the maximum and minimum errors are 0.8 m/s and -0.8 m/s, respectively, in the case of the WRF wind direction, whereas these errors are -1.6 m/s and -1.6 m/s, respectively, in the case of the NCEP FNL wind direction. On the whole, the wind direction with a larger MAE tends to yield a larger magnitude of error for wind speed. However, in some ranges of wind direction, the relation reverses, and a less accurate wind direction can lead to a more accurate wind speed. For instance, the NCEP NFL wind direction, which has the largest MAE, has a more accurate wind speed at wind direction of around 60 °, 140 °, 230 ° and 320 °. The reverse order of the accuracy of the wind speeds calculated by the MANAL and QuikSCAT wind directions can be interpreted as being a case such as that shown in Figure 3.7.

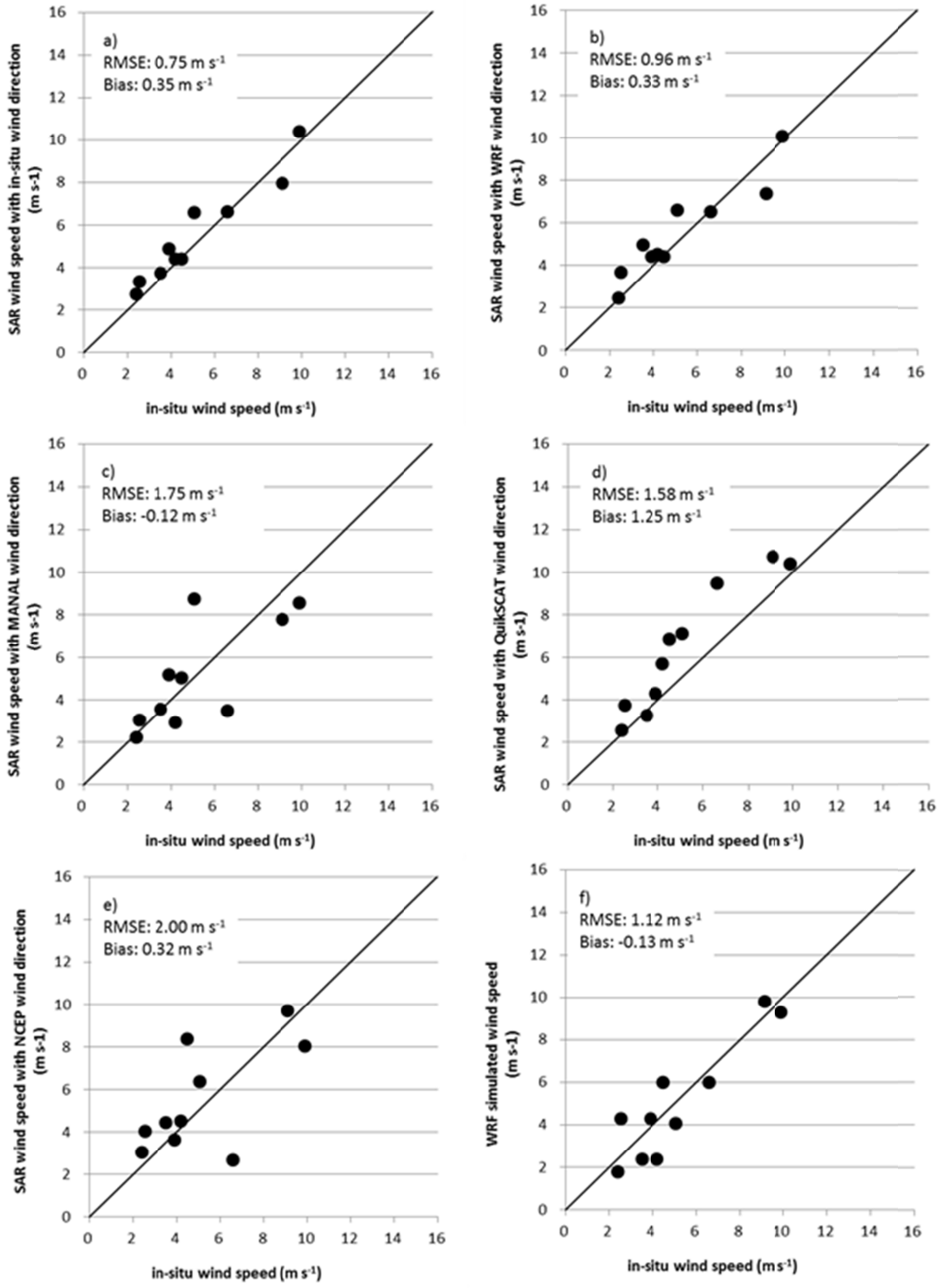

Figure 3.6 Relation between the *In-situ* wind speed and the SAR wind speed retrieved by CMOD5.N using wind directions: (a) *In-situ*, (b) WRF, (c) MANAL, (d) QuikSCAT and (e) NCEP FNL in the case of onshore wind only. An accuracy of WRF wind speeds is also shown in (f)

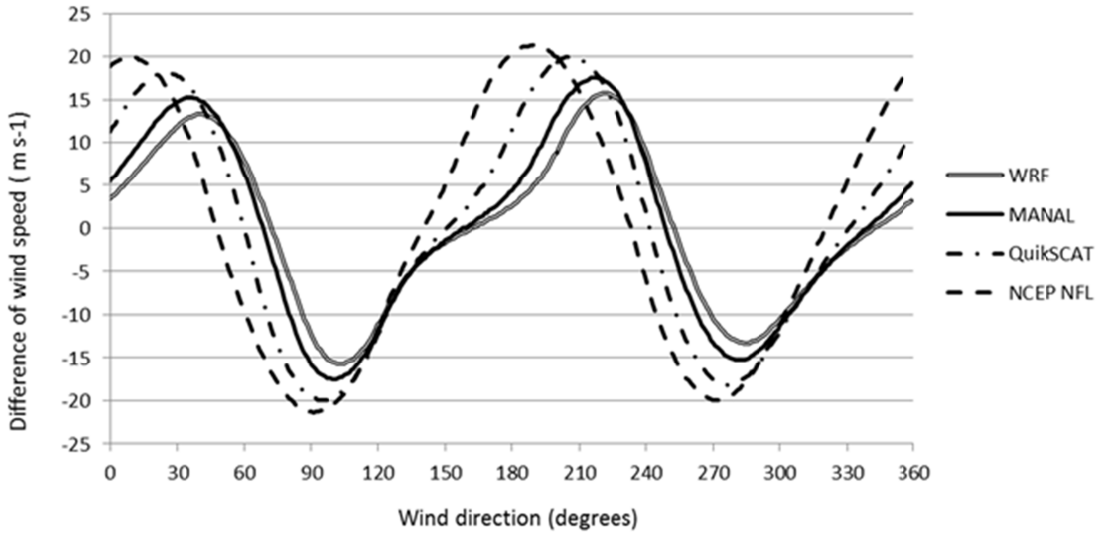

Figure 3.7 Differences in CMOD5.N-retrieved wind speeds between a given wind direction and the given wind direction plus the MAE of each external wind direction. The NRCS and incidence angle are assumed as 0.0 dB and 20.0 °, respectively.

3.3.4 Discussion on uncertainty arising from the small number of samples

The effectiveness of using the WRF wind direction in the SAR wind speed retrieval is supported by a small number of samples, although the effectiveness is partly confirmed in the previous section. When the SAR-retrieved wind speed is directly validated with respect to the *In-situ* wind speed, the SAR and *In-situ* data have to be selected for corresponding times and locations. It is not easy to use a large number of samples in this context. In this section, the uncertainty in the estimated RMSE arising from the small number of samples is discussed.

In order to evaluate the uncertainty in the estimated RMSE, the 95% confidence interval in the RMSE is applied. First, the relationship among the variance (σ^2), RMSE and bias is obrtained from the definition of the variance presented by Sheiner and Beal (1981):

$$\begin{aligned}\sigma^2 &= \frac{1}{N}\sum_{i=1}^{N}\left(x_i - y_i - \frac{1}{N}\sum_{i=1}^{N}(x_i - y_i)\right)^2 \\ &= \frac{1}{N}\sum_{i=1}^{N}(x_i - y_i)^2 - \left(\frac{1}{N}\sum_{i=1}^{N}(x_i - y_i)\right)^2 \\ &= RMSE^2 - Bias^2\end{aligned} \tag{3.8}$$

Where the RMSE can be obtained as

$$RMSE = \sqrt{\sigma^2 + Bias^2} \tag{3.9}$$

Normally, the variance follows a chi-squared (χ^2) distribution, and the α% confidence interval in variance is given as

$$\frac{NS^2}{\chi^2_{N-1}\left(\frac{\alpha}{2}\right)} < \sigma^2 < \frac{NS^2}{\chi^2_{N-1}\left(1-\frac{\alpha}{2}\right)} \tag{3.10}$$

where, S^2 is the sampling variance. The bias follows a t-distribution (T), and the α% confidence interval in bias is obtained as

$$\frac{1}{N}\sum_{i=1}^{N}(x_i - y_i) - T_\alpha\frac{S}{\sqrt{N}} < Bias < \frac{1}{N}\sum_{i=1}^{N}(x_i - y_i) + T_\alpha\frac{S}{\sqrt{N}} \tag{3.11}$$

Thus the α% confidence interval of the RMSE is given as

$$\begin{aligned}&\sqrt{\frac{NS^2}{\chi^2_{N-1}\left(\frac{\alpha}{2}\right)} + \left(\frac{1}{N}\sum_{i=1}^{N}(x_i - y_i) - T_\alpha\frac{S}{\sqrt{N}}\right)^2} < RMSE < \sqrt{\frac{NS^2}{\chi^2_{N-1}\left(1-\frac{\alpha}{2}\right)} + \left(\frac{1}{N}\sum_{i=1}^{N}(x_i - y_i) + T_\alpha\frac{S}{\sqrt{N}}\right)^2} \quad (B_{\min} > 0) \\ &\sqrt{\frac{NS^2}{\chi^2_{N-1}\left(\frac{\alpha}{2}\right)}} < RMSE < \sqrt{\frac{NS^2}{\chi^2_{N-1}\left(1-\frac{\alpha}{2}\right)} + \left(\frac{1}{N}\sum_{i=1}^{N}(x_i - y_i) + T_\alpha\frac{S}{\sqrt{N}}\right)^2} \quad (B_{\min} < 0, |B_{\min}| < |B_{\max}|) \\ &\sqrt{\frac{NS^2}{\chi^2_{N-1}\left(\frac{\alpha}{2}\right)}} < RMSE < \sqrt{\frac{NS^2}{\chi^2_{N-1}\left(1-\frac{\alpha}{2}\right)} + \left(\frac{1}{N}\sum_{i=1}^{N}(x_i - y_i) - T_\alpha\frac{S}{\sqrt{N}}\right)^2} \quad (B_{\min} < 0, |B_{\min}| > |B_{\max}|)\end{aligned} \tag{3.12}$$

where, B_{max} and B_{min} are the minimum and minimum values, respectively, of the α% confidence interval in the bias. However in order to simplify the calculations, Sheiner *et al*. (1981) did not consider the bias.

The 95% confidence intervals in the RMSE with six types of wind directions

data (*In-situ*, WRF, No info, MANAL, QuikSCAT and NCEP FNL) for 42 SAR images are shown in Figure 3.8(a). The uncertainty interval with the WRF wind direction as well as that for MANAL, QuikSCAT, and No information ranges from 1.5 m/s to nearly 3 m/s. This large interval can occur for two reasons: the small number of samples and the relatively low dependency of the SAR-retrieved wind speed on wind direction, as the winds are low to moderate. However, in the case of onshore wind (Figure 3.8b)), the uncertainty interval with the WRF wind direction is narrow at around 1 m/s despite the very low number of samples. The RMSE of 0.96 m/s reported earlier for wind speed using the WRF wind direction is the comparable in order of magnitude of the uncertainty at the 95% confidence level. This result verifies that a dependency of the SAR-retrieved wind speed on wind direction is found for the onshore cases. Moreover, the WRF wind direction, which has the highest accuracy of the external wind directions, yields the smallest RMSE in SAR wind speed in the case of only onshore wind. Thus, the dependency of the SAR-retrieved wind speed on wind direction cannot be ignored, although error factors of offshore winds (e.g., fetch, shallow water depth, coastline, land on the wind ward side etc.) appear to add larger errors than wind directions. In the future plan, validation using a large number of samples is suggested in order to increase the reliability of the effectiveness of the WRF wind direction. According to Barthelmie and Pryor (2003) it is necessary to have approximately 60 to 70 samples are necessary in order to estimate the mean wind speed to within +/- 10% at the 90% confidence level.

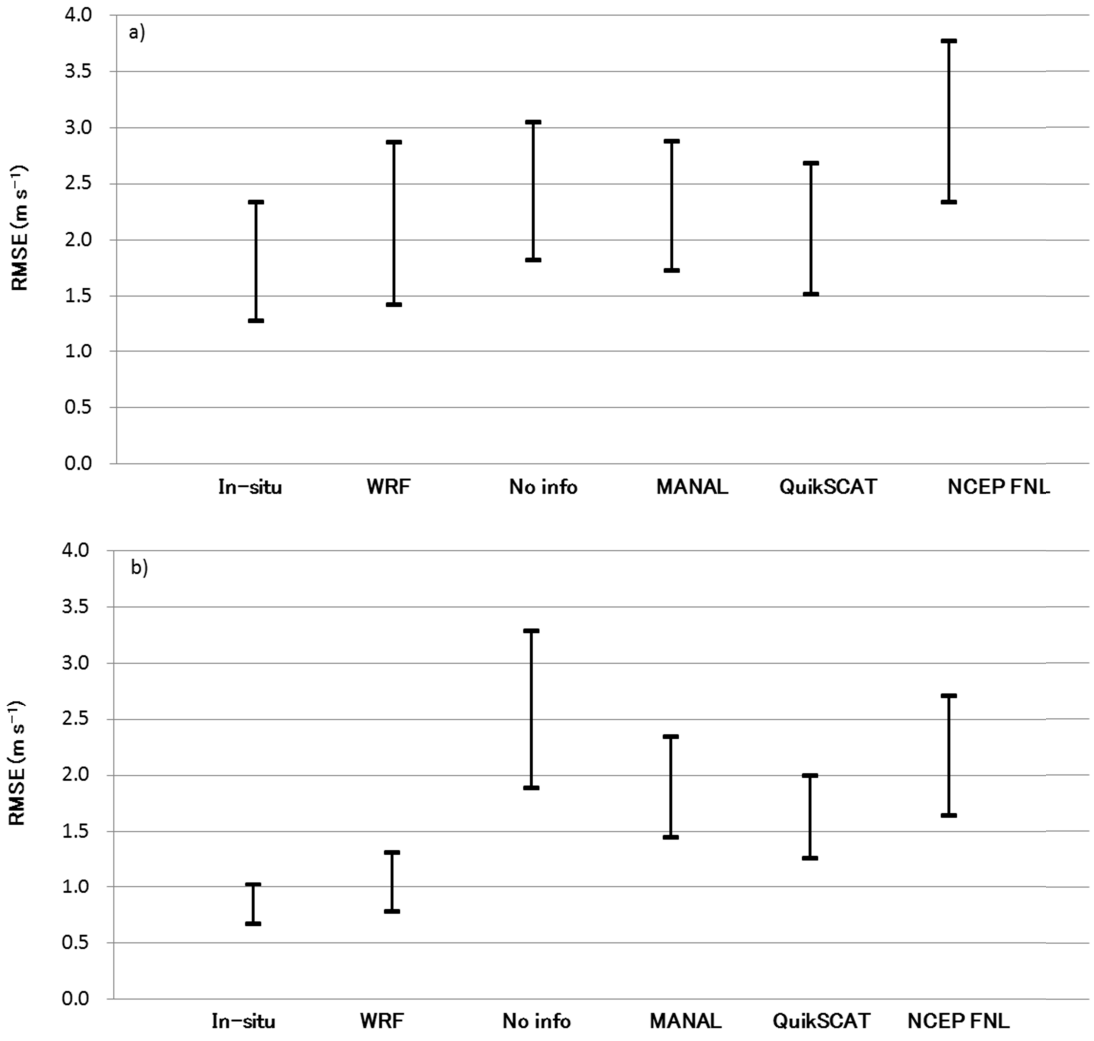

Figure 3.8 The 95% conference intervals of RMSE in SAR-retrieved wind speed obtained using six types of wind direction data (*In-situ*, WRF, No info, MANAL, QuikSCAT, and NCEP FNL): a) both offshore and onshore wind and b) only onshore wind.

3.4 Conclusions

In order to examine the effectiveness of the use of the WRF wind direction for sea surface wind speed retrieval from SAR images in coastal waters, the SAR-retrieved wind speed is validated with respect to the *In-situ* measured wind speed at the Shirahama offshore platform in Japan. The results of the present study are as follows:

1) The RMSE of the wind speeds retrieved from 42 ENVISAT ASAR images with CMOD5.N with the input of the WRF wind direction is 2.15 m/s. This value lies between the RMSE values for the cases of using the *In-situ* wind direction (1.71 m/s) and that of using no information on wind direction (2.24 m/s). However the uncertainty is high at around 2 to 3 m/s at the 95% confidence level due to the small number of samples and additional factors.
2) One of the additional factors is the complex coastline only 2 km away from the meteorological tower. Selecting onshore cases only yields a RMSE of 0.96 m/s using the WRF wind direction. The number of samples is very small but the uncertainty is reduced to 1 m/s at the 95% confidence level.
3) Another aspect of the analysis on the sensitivity of CMOD5.N to wind direction input from *In-situ*, WRF, MANAL, QuikSCAT and NCEP FNL for the site shows that the retrieved wind speed is not greatly affected by the wind direction input because the site is dominated by low winds (The mean wind speed is 7 m/s in the present study).
4) Thus, although the effectiveness of using the accurate WRF wind direction in the SAR wind retrieval is partly confirmed, further efforts to remove error factors other than wind direction, which are peculiar to the vicinity of coastlines are necessary for more accurate SAR wind retrieval in coastal waters.

References

Barthelmie, R. J.; Pryor, S. C. Can satellite sampling of offshore wind speeds realistically represent wind speed distributions? Journal of Applied Meteorology and Climatology, **2003**, *42*, 83–94.

Badger, M.; Badger, J.; Nielsen, M.; Hasager C. B.; Peña, A. Wind class sampling of satellite SAR imagery for offshore wind resource mapping. *Journal of Applied Meteorology and Climatology.* **2010,** *49*, 2474-2491.

Beaucage P.; Glazer A.; Choisnard J.; Yu W.; Bernier M.; Benoit R.: Lafrance, G. Wind assessment in a coastal environment using Synthetic Aperture Radar satellite imagery and a numerical weather prediction model. *Canadian Journal of Remote Sensing*, **2007**, *33*, 5, 368-377, DOI: 10.5589/m07-043.

Beaucage, P.; Bernier, M.; Lafrance, G.; Choisnard, J. Regional Mapping of the Offshore Wind Resource: Towards a Significant Contribution From Space Borne Synthetic Aperture Radars. *IEEE Journal of Selected Topics in Applied Earth Observations and Remote Sensing,* **2008**, *1*, 1, 48-56. DOI: 10.1109/JSTARS.2008.2001760.

Cressman, G. P. An operational objective analysis system. *Monthly Weather Review*, **1959**, *87*, 367-374. DOI: 10.1175/1520-0493.

Du, Y.; Vachon, P.; Wolf, J. Wind direction estimation from SAR images of the ocean using wavelet analysis. *Canadian Journal of Remote Sensing*, **2002,** *28*, 498-509.

Fetterer, F.; Gineris, D.; Wackerman, C. Validating a scatterometer wind algorithm for ERS-1 SAR. *IEEE Trans. Geosci. Remote Sens.,* **1998**, *36*, 479–492. DOI: 10.1109/36.662731.

Gerling, T. W. Structure of the surface wind field from the Seasat SAR. *Journal of Geophys. Res*., **1986**, *91*, C2, 2308-2320. DOI: 10.1029/JC091iC02p02308.

Hasager, C. B.; Furevik, B. R. Validation of ERS-2 SAR offshore wind-speed maps in

the North Sea. *International Journal of Remote Sensing.* **2004**, *25*, 3817-3841. DOI: 10.1080/01431160410001688286.

Hasager, C. B.; Barthelmie, R. J.; Christiansen, M. B.; Nielsen, M.; Pryor, S. C. Quantifying Offshore Wind Resources from Satellite Wind Maps: Study Area the North Sea. *Wind Energy* **2006**, *9*, 63–74. DOI: 10.1002/we.190.

Hasager, C. B.; Badger, M.; Peña, A.; Larsén, X.G.; Bingöl, F. SAR-Based Wind Resource Statistics in the Baltic Sea, *Remote Sens.* **2011**, *3*, 117-144, DOI: 10.3390/rs3010117.

Hersbach, H. Comparison of C-Band Scatterometer CMOD5.N Equivalent Neutral Winds with ECMWF. *Journal of Atmospheric and Oceanic Technology*, **2010**, *27*, 721–736. DOI: 10.1175/2009JTECHO698.1.

Horstmann, J.; Lehner, S.; Koch, W.; Tonboe, R. Computation of wind vectors over the ocean using spaceborne Synthetic Aperture Radar. *Johns Hopkins APL Technical Digest*, **2000**, *21*, 1.

Horstmann, J.; Koch, W.; Lehner, S.; Tonboe, R. Wind retrieval over the ocean using Synthetic Aperture Radar with C-band HH Polarization. *IEEE Trans. Geosci. Remote Sens.* **2000,** *38*, 5, 2122 – 2131. DOI: 10.1109/36.868871.

Horstmann, J.; Koch, S.; Leher, S.; Toeboe, R. Ocean winds from RADARSAT-1 ScanSAR. *Canadian Journal of Remote Sensing*, **2002,** *28*, 524-533.

Koch, W. Directional analysis of SAR images aiming at wind direction. *IEEE Trans. Geosci. Remote Sens.* **2004**, *42*, 4, 2587-2600. DOI: 10.1109/TGRS.2003.818811

Kozai, K.; Ohsawa, T.; Shimada, S.; Takeyama, T.; Hasager, C. B.; Badger, M. Comparison of ENVISAT/ASAR-estimated offshore wind resource maps around Shirahama with those from mesoscale models MM5 and WRF. *Proceedings of the European Offshore Wind Conference,* **2009**.

Lehner, S.; Horstmann, J.; Koch, W.; Rosenthal, W. Mesoscale wind measurements using recalibrated ERS SAR images. *Journal of Geophys. Res.*, **1998,** *103*, C4, 7847-7856. DOI: 10.1029/97JC02726.

Liu, W. T.; Katsaros, K.B.; Businger, J.A. Bulk parameterization of air-sea exchanges of heat and water vapor including the molecular constraints at the Interface. *J. Atmos. Sci.*1979, *36*, 1722–1735.

Liu, W. T.; Tang, W. Equivalent Neutral Wind, *JPL publication,* **1996**, *96-17*, 8pp.

Monaldo, F., Thompson, D., Beal, R., Pichel, W., Clemente-Colón, P., Comparisons of SAR-derived wind speed with model predictions and ocean buoy measurements. *IEEE Transaction on Geoscience and Remote Sensing*. **2001**, *39*, 12: 2587-2600. DOI: 10.1109/36.974994.

Sheiner L. B.; Beal, S. L. Some suggestions for measuring predictive performance. *Journal of Pharmacokinetics and Pharmacodynamics*. **1981**, *9*, 4, 503-512. DOI: 10.1007/BF01060893.

Shimada, T.; Kawamura, H.; Shimada, M.; Iwasaki, S. Evaluation of JERS-1 SAR images from a coastal wind retrieval point of view. *IEEE Transaction on Geoscience and Remote Sensing*, **2004**, *42*, 3: 491-500. DOI: 10.1109/TGRS.2003.821268.

Takeyama, Y.; Ohsawa, T.; Kozai, K. Estimation of coastal wind fields by synthetic aperture radar and mesoscale meteorological model. *Proceedings of Renewable Energy* **2006**; Chiba, Japan.

Vachon, P. W.; Dobson, F. W. Validation of wind vector retrieval from ERS-1 SAR images over the ocean. *The Global Atmosphere and Ocean System*, **1996**, *5*, 177-187.

Vachon, P. W.; Dobson, F. W. Wind retrieval from RADARSAT SAR images: selection of a suitable C-band HH polarization wind retrieval model. *Canadian Journal of Remote Sensing*, **2000**, *26*, 306-313.

Wackerman, C.; Rufenach, C.; Shuchman, R.; Johannessen, J. Davidson, K. Wind vector retrieval using ERS-1 Synthetic Aperture Radar imagery. *IEEE Transaction on Geosciences and Remote Sensing*, **1996**, *34*, 1343-1352. DOI: 10.1109/36.544558.

Wackerman, C.; Pichel, W.; Li, X.; Clemente-Colon, P. Estimation of surface winds from SAR using a projection algorithm. *Proceedings of the 14th Conference on Satellite Meteorology and Oceanography*, **2006**, J4.4.

Chapter 4

Estimation of offshore wind resources in coastal waters off Shirahama using ENVISAT Advanced SAR images

4.1 Introduction

From the satellite-borne Synthetic Aperture Radar (SAR) it is possible to retrieve a sea surface wind speed field with a high spatial resolution of tens to hundreds of meters, and it is thus expected that the SAR image can be used for wind resource assessment in coastal waters. In fact, the offshore wind resource assessment using SAR has been conducted in many places, especially in Europe (Hasager *et al*., 2011, Christiansen et al., 2006, Hasager *et al.*, 2004).

On the other hand, in Japan, since there has been little need for offshore wind resource assessment at least up to the accident of the Fukushima nuclear power plant, there are few papers in which offshore wind resource is practically assessed with SAR, except some preliminary papers like Kozai *et al*. (2009a). But now, offshore wind energy is gradually regarded as a promising electric power resource, and there is increased need for assessing the offshore wind resource. It is thus desirable that the SAR-based offshore wind resource assessment, which is reported to work well in European seas, could also be applicable to Japanese coastal waters. However, compared to the European seas such as the North Sea, Japanese coastal waters have more complex coastlines and onshore terrains as well as they are affected by non-neutral atmospheric stability due to the Kuroshio Current. In fact, the authors have found that the performance and accuracy of the SAR-based wind speed estimation method are different between Europe and Japan, and thus have investigated how to use SAR for offshore wind resource assessment in Japanese coastal waters (Takeyama *et al.* 2012, Takeyama *et al*., 2013, Kozai *et al.*, 2009).

First, Takeyama *et al*. (2012) discussed the wind directions used as input to a geophysical model function (GMF) to derive 10 m-height wind speed from a SAR image. As a result, it was found that estimated wind speed became the most accurate

when using a high resolution wind direction field output from numerical simulation with the mesoscale meteorological model WRF (Weather Research and Forecasting model) (Skamarock *et al.,* 2008). Thus, this study uses the WRF wind direction as input to GMF. Secondly, Takeyama *et al*. (2013) compared the performances of four GMFs: CMOD4, CMOD5, CMOD_IFR2 and CMOD5.N (Hersbach *et al*., 2010) at two sites in Japanese coastal waters and concluded that CMOD5.N, which can correct the effect of atmospheric stability, retrieves the most accurate wind speeds of the four. Thus, the latest GMF CMOD5.N is used to derive wind speed from SAR images. Thirdly, it is generally believed that a larger number of SAR images leads to a higher accuracy of the assessment. Kozai *et al*. (2009a) examined the number of SAR images necessary to estimate long-term mean wind speed at Shirahama, and concluded that at least 74 to 128 SAR images are required when assuming a 10% error and 90% confidence interval. The number is a little bit larger than that of Barthelmie and Pryor (Barthelmie and Pryor, 2010), to which Kozai *et al.* (2009b) referred, reporting that 60 to 70 randomly selected images are required to characterize the mean wind speed and Weibull distribution scale parameter, and nearly 2,000 images are needed to obtain energy density. According to these results, the number of 104 SAR images, used in this study, can be considered to be almost sufficient for mean wind speed estimation, but it might be insufficient for wind energy density estimation.

This study aims at two things. One is to examine the accuracy of offshore wind resource estimation (long-term mean wind speed and wind energy density) using SAR images and the Weibull analysis, and the other is to finally make wind resource maps in the coastal waters off Shirahama. The methods of wind speed estimation from SAR images, comparison with *In-situ* measurements, and application of the Weibull distribution function are described in Subsection 4.2. Accuracies of SAR-derived wind speeds and Weibull parameters are examined in Subsections 4.3.1 and 4.3.2, respectively. Subsection 4.3.3 describes the way to make the offshore wind resource maps, which are finally presented at the end of this paper.

4.2 DATA and Methods

4.2.1 Target area and In-situ measurements

The target area of the study in this section is the coastal waters off Shirahama, shown in Figure 4.1. This area is located in the western part of Japan, including the Kii Channel facing the Pacific Ocean, and known as a relatively windy coastal area in this region, because this channel gives passage to the northwesterly winter monsoon wind. In this area there are two observation sites; the Shirahama offshore platform and the South Wakayama buoy (Hereinafter, SW-buoy). The first one, the Shirahama offshore platform (33°42'32"N, 135°19'58"E) is the oceanographic and meteorological observation station operated by the Disaster Prevention Research Institute, Kyoto University since 1994. On the platform, wind speed and direction are measured at a height of 23 m above mean sea level with a propeller anemometer. This study uses the hourly 10-minute averaged wind speed from 2003 to 2011. The second one, the SW-buoy (33°38'32"N, 135°09'24"E) is a buoy for wave observation and is operated by the Ports and Harbors Bureau, Ministry of Land, Infrastructure, Transport and Tourism. On the buoy, wind speed and direction are measured with a propeller anemometer at a height of 7 m. The hourly 10-min averaged wind speed data for two years from 2009 to 2010 is used in this study.

In order to compare the SAR-derived wind speed at 10 m height with *In-situ* measured wind speeds, the *In-situ* wind speeds at 23 m height at Shirahama is corrected to the 10 m-height wind speed. For this height correction, the LKB code (Liu *et al.*, 1979), which can calculate vertical profile of wind speed based on the Monin-Obukhov similarity theory, is used. Three kinds of inputs; air temperature, relative humidity, and sea surface temperature (SST) are required in the LKB code. Here, these parameters are acquired from the mesoscale meteorological mode (WRF). The wind profile, which can take the effect of atmospheric stability expressed as $\Psi_u(\zeta)$ into account, is shown as

$$u = \frac{u_*}{\kappa}\left[ln\left(\frac{z}{z_0}\right) - \Psi_u(\zeta)\right] \tag{4.1}$$

Here, u_* is frictional velocity, z_0 is roughness length, and κ is the von Karman constant (=0.4). The relation between z_0 and u_* is given as

$$z_0 = 0.11\frac{\nu}{u_*} + \alpha\frac{u_*^2}{g} \tag{4.2}$$

where α is Charnock's parameter with a value of 0.011 (Charnock, 1955), υ is the kinematic viscosity, and g is the acceleration due to gravity. The parameters, z_0 and u_* can be determined iteratively through the Equations (4.1) and (4.2) and other equations regarding the stability parameter ζ. In the height correction from 23 m to 10 m, wind speed is decreased by 5% on average. The converted 10 m-height 10-min averaged wind speeds are used as the *In-situ* values for the comparison with the SAR-derived wind speeds.

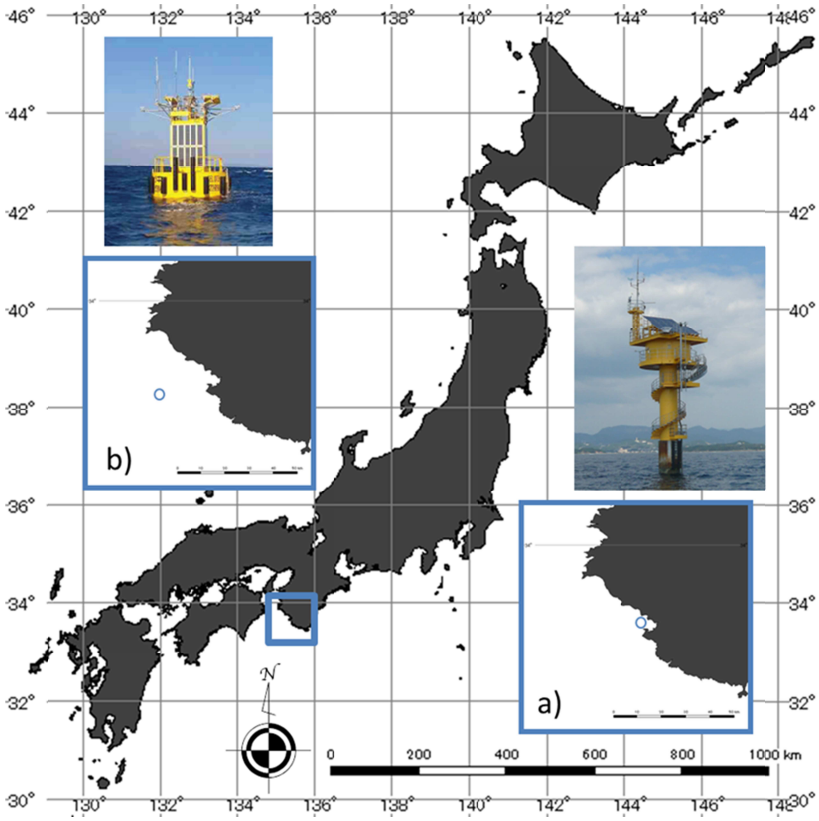

Figure 4.1 Locations of the coastal waters off Shirahama. Circle in the small maps indicates (a) the Shirahama offshore platform and (b) the Southwest Wakayama buoy (SW-buoy).

4.2.2 Derivation of wind speed from SAR image

Figure 4.2 shows the flow chart of how to assess offshore wind resource using SAR images. In-depth descriptions regarding each processing will be given later.

Firstly, this study uses 104 images from the C-band ASAR onboard the ENVISAT satellite, launched by the European Space Agency in 2002. The inventory of the SAR data used here is listed in Table 4.1. They include two kinds of images; the Precision Image Product (IMP) and the Wide Swath Mode (WSM). The IMP and WSM images have 12.5 m and 75 m pixel spacing, respectively. But in the preprocessing these SAR images are smoothed to the grids with a 0.005 × 0.005 degree spatial resolution to remove the speckle noise, which is appeared in coherent imaging systems such as SAR.

For deriving wind speed from the SAR image, CMOD5.N (Hersbach, 2010) is used to derive wind speed from normalized radar cross section (NRCS) represented in the SAR images. The primary equation of CMOD5.N can be written as

$$\sigma_{vv}^{o} = b_0\left(1.0 + b_1\cos\phi + b_2\cos(2\phi)\right)^{1.6}, \tag{4.3}$$

where σ_{vv}^{0} is the VV-polarized NRCS obtained from a SAR image, ϕ is the relative wind direction defined as the angle between the radar look direction and true wind direction, and b_0, b_1, and b_2 are the parameters depending on the radar incidence angle and wind speed. Here, it is necessary to acquire values of wind direction from another external data source. Being similar to Takeyama *et al*. (2012), this study uses the wind direction obtained from numerical simulation with the mesoscale meteorological model WRF (Skamarock *et al*., 2008). Details of the WRF simulation are described in Subsection 4.2.3.

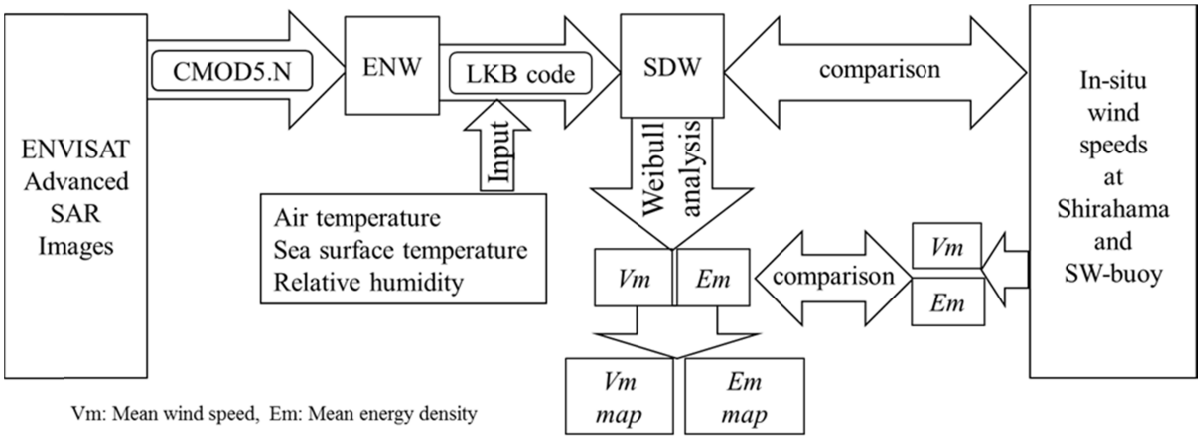

Figure 4.2 Flowchart of wind resource estimation from Advanced SAR images and their comparison with *In-situ* measurements.

Table 4.1 Inventory of 113 ENVISAT Advanced SAR images used in this study.

Date (year/month/day)	Time (hour: min: sec)	Ascending or Descending	Observation mode	Date (year/month/day)	Time (hour: min: sec)	Ascending or Descending	Observation mode
20030207	01:06:54	DS	IMP	20100624	12:50:44	AS	WSM
20030314	01:06:56	DS	IMP	20100625	01:06:07	DS	WSM
20030418	01:06:59	DS	IMP	20100627	12:56:29	AS	WSM
20030507	01:09:47	DS	IMP	20100630	13:02:14	AS	WSM
20030611	01:09:47	DS	IMP	20100708	00:57:30	DS	WSM
20030716	01:09:53	DS	IMP	20100710	12:47:52	AS	WSM
20030801	01:07:05	DS	IMP	20100711	01:03:15	DS	WSM
20030820	01:09:56	DS	IMP	20100713	12:53:38	AS	WSM
20030924	01:09:56	DS	IMP	20100724	00:54:39	DS	WSM
20031010	01:07:04	DS	IMP	20100726	12:45:02	AS	WSM
20031029	01:09:50	DS	IMP	20100727	01:00:25	DS	WSM
20031114	01:07:01	DS	IMP	20100730	01:06:10	DS	WSM
20031219	01:07:03	DS	IMP	20100801	12:56:32	AS	WSM
20040123	01:07:00	DS	IMP	20100812	00:57:33	DS	WSM
20040211	01:09:51	DS	IMP	20100814	12:47:55	AS	WSM
20040227	01:07:00	DS	IMP	20100815	01:03:18	DS	WSM
20040317	01:09:54	DS	IMP	20100817	12:53:40	AS	WSM
20040507	01:07:00	DS	IMP	20100818	01:09:03	DS	WSM
20040630	01:09:55	DS	IMP	20100828	00:54:41	DS	WSM
20040731	12:48:26	AS	IMP	20100830	12:45:03	AS	WSM
20040820	01:07:04	DS	IMP	20100831	01:00:26	DS	WSM
20040908	01:09:55	DS	IMP	20100903	01:06:10	DS	WSM
20041013	01:09:56	DS	IMP	20100905	12:56:32	AS	WSM
20041029	01:07:06	DS	IMP	20100916	00:57:32	DS	WSM
20041113	12:48:22	AS	IMP	20100918	12:47:54	AS	WSM
20041117	01:09:54	DS	IMP	20100919	01:03:17	DS	WSM
20041203	01:07:03	DS	IMP	20100921	12:53:38	AS	WSM
20050107	01:06:58	DS	IMP	20100922	01:09:01	DS	WSM
20050211	01:07:01	DS	IMP	20111018	12:58:01	AS	WSM
20050511	01:09:59	DS	IMP	20111019	01:11:12	AS	WSM
20050527	01:07:07	DS	IMP	20111026	13:04:41	AS	WSM
20050701	01:07:09	DS	IMP	20111029	12:54:47	AS	WSM
20050805	01:07:05	DS	IMP	20111030	01:07:59	DS	WSM
20050909	01:07:02	DS	IMP	20111106	13:01:28	AS	WSM
20051014	01:07:05	DS	IMP	20111109	12:51:34	AS	WSM
20051118	01:07:03	DS	IMP	20111114	13:08:08	AS	WSM
20051223	01:06:57	DS	IMP	20111125	13:04:54	AS	WSM
20060111	01:09:42	DS	IMP	20111206	13:01:39	AS	WSM
20060215	01:09:45	DS	IMP	20111207	01:14:50	AS	WSM
20060303	01:06:54	DS	IMP	20111209	12:51:45	AS	WSM
20070829	01:09:47	DS	IMP	20111210	01:04:56	DS	WSM
20071107	01:09:43	DS	IMP	20111214	13:08:19	AS	WSM
20071123	01:06:48	DS	IMP	20111217	12:58:25	AS	WSM
20071208	12:48:10	AS	IMP	20111218	01:11:36	AS	WSM
20071209	01:03:59	DS	IMP	20111221	01:01:42	DS	WSM
20071212	01:09:41	DS	IMP	20111228	12:55:10	AS	WSM
20071227	12:51:02	AS	IMP	20120105	13:01:49	AS	WSM
20071228	01:06:50	DS	IMP	20120106	01:15:00	AS	WSM
20080112	12:48:12	AS	IMP	20120108	12:51:55	AS	WSM
20080113	01:04:01	DS	IMP	20120109	01:05:05	DS	WSM
20080116	01:09:43	DS	IMP	20120113	13:08:26	AS	WSM
20080131	12:51:01	AS	IMP	20120116	12:58:33	AS	WSM
20080201	01:06:50	DS	IMP				
20080216	12:48:09	AS	IMP				
20080217	01:03:59	DS	IMP				
20080220	01:09:42	DS	IMP				
20080306	12:51:02	AS	IMP				
20080307	01:06:51	DS	IMP				
20080322	12:48:13	AS	IMP				
20080323	01:04:02	DS	IMP				
20080326	01:09:43	DS	IMP				

4.2.3 Conversion from equivalent wind speed (ENW) to stability-dependent wind speed (SDW)

The output from CMOD5.N is the equivalent neutral wind speed (ENW) (Liu *et al*., 1996), which is the wind speed obtained under the assumption of neutral atmospheric stability in the surface layer. Thus, the LKB code (Liu *et al*., 1979) is used to convert the ENW to the stability-dependent wind speed (SDW), which is comparable to a true wind speed. Since Takeyama *et al.* (2013) provides an in-depth description of how to calculate SDW from ENW with the LKB code. What is important is that the LKB code requires three parameters; air temperature, relative humidity, and sea surface temperature (SST) to calculate SDW, and this study obtains these three values from numerical simulation with the mesoscale meteorological model WRF.

The WRF (Weather Research and Forecasting model, http://www.mmm.ucar.edu/wrf/users/docs/arw_v3.pdf) is the mesoscale numerical weather prediction system developed by seven institutes in the United States including the National Center for Environmental Prediction (NCEP) and the National Center for Atmospheric Researches (NCAR). In this study, WRF is set up with two domains consisting of 100 × 100 grids with horizontal resolutions of 5 km and 1 km, and 28 vertical layers. As the initial and boundary conditions, 3-hourly (6-hourly before February 2006) 5 km × 5 km (10 km × 10 km before April 2009) mesoscale analysis MANAL provided from Japan Meteorological Agency and daily 0.05° × 0.05° sea surface temperature OSTIA SST provided from Met Office (http://ghrsst-pp.metoffice.com/pages/latest_analysis/) are used in the simulation. WRF is run for 24 h for each SAR image, corresponding to the time of passage of ENVISAT (mostly at 01 and 13 UTC) with two-way nesting, which allows the interaction between the mother and child domains. More in-depth model configuration is shown in Table 4.2, and the domains used in the WRF simulation are shown in Figure 4.3. In the previous study (Takeyama *et al.*, 2013), a root mean square error (RMSE) of the wind direction from the WRF simulation was reported as 25.4° at Shirahama.

Table 4.2 Configurations of the mesoscale meteorological model WRF and input data.

Initial data		JAM Meso-Analysis (MANAL) 5 km × 5 km, 10 km × 10 km (before April 2009) 3-hourly, 6-hourly (before February 2006) Met Office OSTIA SST (0.05° × 0.05°, daily)	
Nesting option		two-way nesting	
Vertical resolution		28 levels (surface to 100 hPa)	
Time period		24 h including the time of passage of ENVISAT	
Domain		Domain 1	Domain 2
Horizaontal resolution		5.0 km	1.0 km
Grid points		100 × 100	101 × 101
Time step		30 s	6 s
Physics option	Surface layer	Monin-Obukhov (Janjic Eta)	
	Planetary Boundary Layer	MYJ (Eta) TKE	
	Short wave radiation	Dudhia	
	Long wave radiation	RRTM	
	Cloud micropysics	WSM3	
	Cumulus parameterization	Kain-Fritsch (new Eta)	none
	Land surface	Five-layer soil	
FDDA option		Enable including PBL	Enable excluding PBL

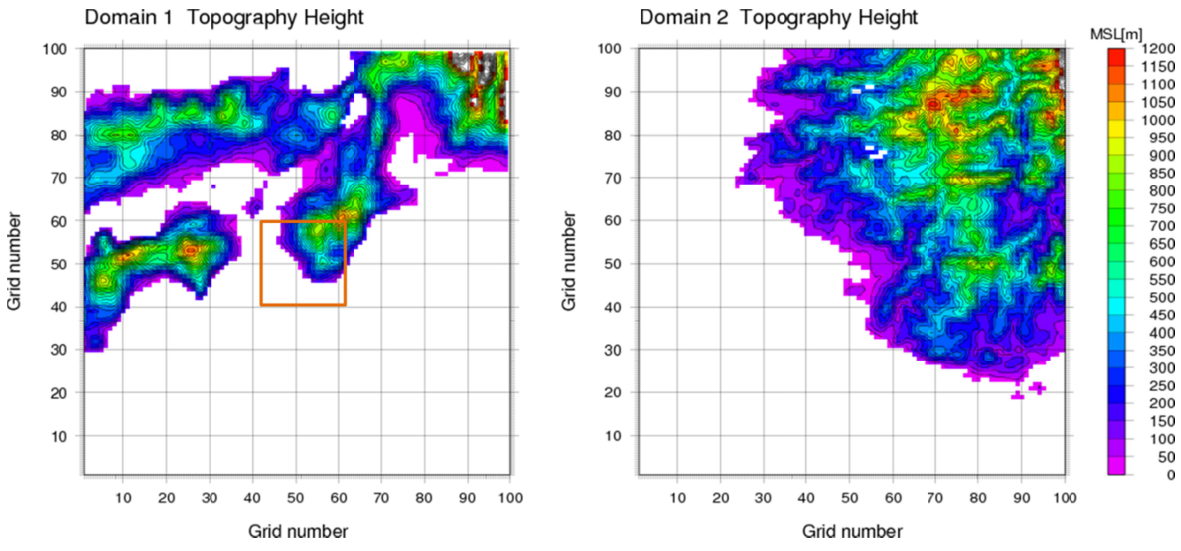

Figure 4.3 Domains used in the WRF simulation.

4.2.4 Application of Weibull distribution function

The wind resource assessment using SAR images is normally accompanied with the use of the Weibull analysis. With the Weibull distribution, the probability density function of wind speed is expressed as the following equation.

$$f(V) = \frac{k}{A}\left(\frac{V}{A}\right)^{k-1} \exp\left[-\left(\frac{V}{A}\right)^{k}\right], \tag{4.4}$$

where V is wind speed (m/s), and k and A are called shape and scale parameters, respectively. From the two parameters k and A, mean wind speed V_m can be calculated as follows;

$$V_m = A\Gamma\left(1+\frac{1}{k}\right). \tag{4.5}$$

Here, Γ is the Gamma function defined as

$$\Gamma\left(1+\frac{1}{k}\right) = \int_0^{\infty} t^{1/k} e^{-t} dt. \tag{4.6}$$

The mean wind energy density E_m is shown as

$$E_m = \frac{\rho}{2} A^3 \Gamma\left(1+\frac{3}{k}\right) \tag{4.7}$$

Here, ρ is air density, which is set to 1.225 (kg/m^3) in this study. In the next section, wind resources are evaluated with the mean wind speed V_m and E_m.

4.3 Results and Discussion

4.3.1 Accuracy of SAR-derived wind speed and wind energy density

First, the accuracy of the SAR-derived wind speed and wind energy density is examined. Figure 4.4 shows scatter plots of SAR-derived *versus In-situ* measured wind speeds. In Figure 4.4, the bias and the RMSE of the SAR wind speed are 0.52 m/s and 2.33 m/s, respectively. Since the mean *In-situ* wind speed is 4.92 m/s, the relative ratios of the bias and RMSE become 11% and 47%, respectively. This result has two different characters from the previous study (Takeyama *et al.*, 2012). Firstly, the result shows a lower accuracy than those in the previous study. One of the reasons for the lower accuracy is low wind speeds (no more than 2 m/s). In the SAR wind speed retrieval, low wind speeds are usually removed because it is well known that GMFs cannot derive these wind speeds with high accuracy. But, in this study, all ranges of wind speeds are included, because they are necessary for an estimation of the Weibull distribution (shown detail in Subsection 4.3.2). Secondly, this result has a positive bias though there are negative biases in the previous study. In this Chapter, ENVISAT/ASAR Image mode precision (IMP) images are not only used but also Wide Swath mode (WSM). The difference between observation modes may lead the difference of a tendency of biases. There is still room for consideration.

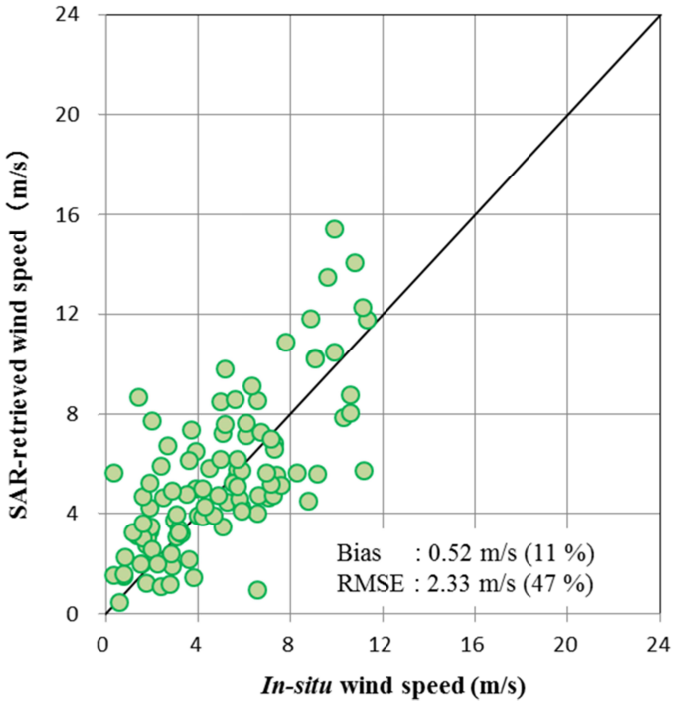

Figure 4.4 Scatter plots of SAR-derived versus measured wind speeds at Shirahama.

4.3.2 Comparisons in terms of Weibull distribution function

Figure 4.5 compares the Weibull distribution for 104 SAR-derived wind speeds at Shirahama with that for corresponding *In-situ* measurements. The scale parameters A are 6.14 (SAR) and 5.52 m/s (*In-situ*), and the shape parameters k are 1.89 (SAR) and 1.74 m/s (*In-situ*). Though the difference of k between them is only 0.15, the difference of A is no less than 0.62 m/s (10%). Meanwhile, mean wind speeds V_m are 5.45 (SAR) and 4.92 m/s (*In-situ*). The difference of V_m is approximately 10%, indicating that the SAR-derived mean wind speed is higher than the *In-situ* measurement. The tendency of the overestimation becomes more remarkable in mean wind energy density E_m. The energy density E_m estimated from the SAR-derived and *In-situ* measured wind speeds exhibits 200 W/m^2 and 162 W/m^2, respectively. The SAR-derived E_m is 24% larger than *In-situ* E_m.

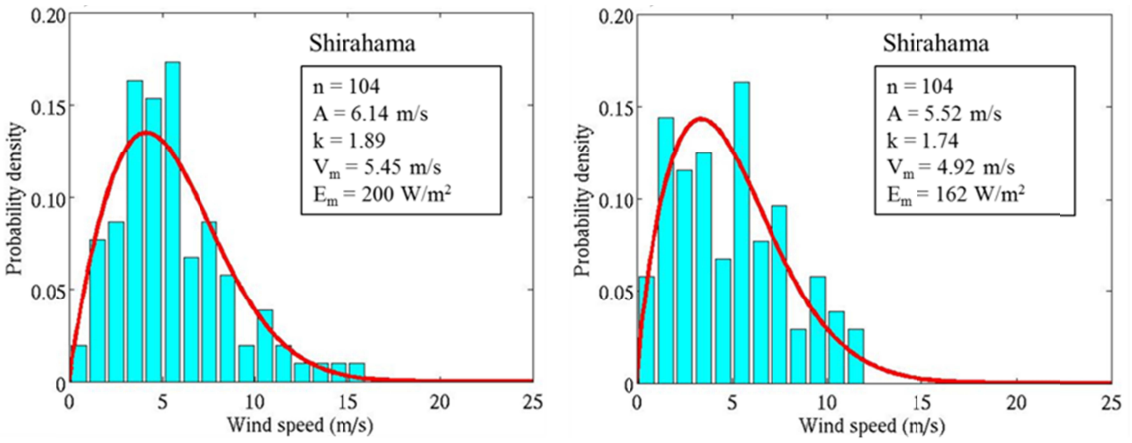

(**a**) SAR (**b**) *In-situ* measurement

Figure 4.5 Comparison of Weibull distributions between (a) SAR-derived and (b) *In-situ* measured wind speeds at Shirahama.

In the next step, the *Vm* and *Em* estimated from SAR images are compared with those from long-term *In-situ* measurement (2003 through 2011) at Shirahama in Figure 4.6. It is firstly confirmed that the differences in both *Vm* and *Em* between Figure 4.6 and Figure 4.5(b) are only 0.16 m/s and 22 W/m^2 and little differences can be seen. This means that the 104 samples well represent characteristics of the long term wind climate. Accordingly, results from the comparison of Figure 4.5(a) with Figure 4.6 are similar to those with Figure 4.5(b). That is, the SAR-estimated *Vm* in Figure 4.5(a) (5.45 m/s) is 1.07 times higher than the long-term mean shown in Figure 4.6 (5.08 m/s). As for mean wind energy density *Em*, the SAR-estimated value is 1.09 times larger than the long-term mean.

Meanwhile, Figure 4.7 compares two Weibull distributions based on SAR and *In-situ* measurements at SW-buoy. At the buoy, 78 SAR images and 16,091 wind speed measurements are used for the comparison. In contrast to Shirahama, the accuracy of the SAR-estimated *Vm* is not good at SW-buoy, and the SAR-estimated *Vm* is 8.51 m/s against the *In-situ* long-term mean of 6.92 m/s. The difference is 23% (1.59 m/s), meaning 1.23 times as large as the *In-situ Vm*. The ratio is slightly larger than that at Shirahama (1.07). Additionally, the mean wind energy density *Em* is 756 W/m^2 for SAR and 414 W/m^2 for *In-situ* measurement, indicating a large overestimation probably due

to the lack of samples, as speculated in the introduction.

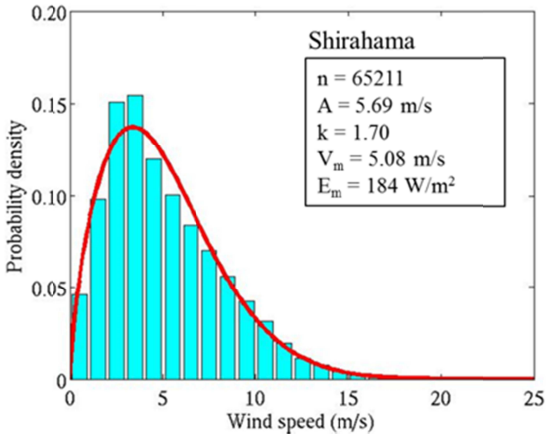

Figure 4.6 Weibull distributions from long-term *In-situ* measured wind speeds (2003 through 2011) at Shirahama.

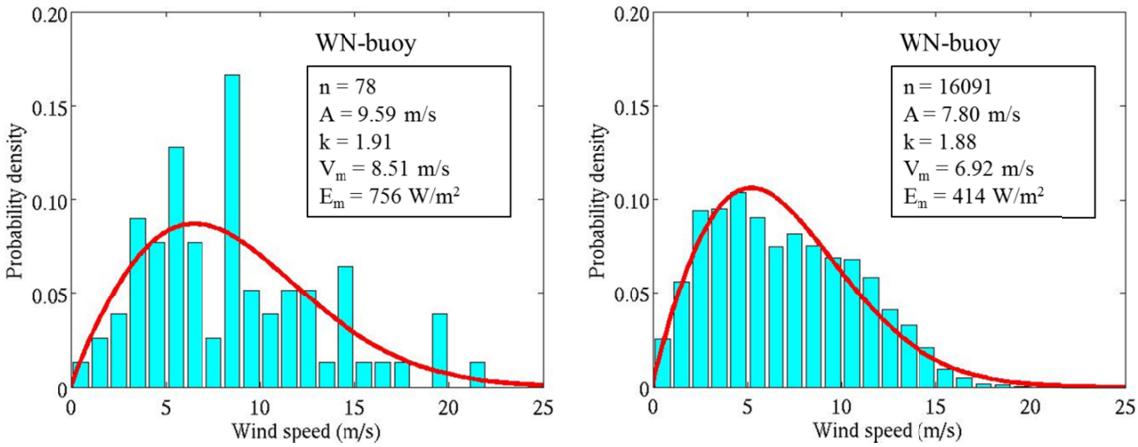

(**a**) SAR (**b**) *In-situ* measurement

Figure 4.7 Comparison of Weibull distributions between (a) SAR-derived and (b) *In-situ* wind speeds at SW-buoy.

4.3.3 Wind resources in coastal waters off Shirahama

The final purpose of this study is to present wind resource maps in the coastal waters off Shirahama. It is desirable that the wind resource maps will be made as accurately as possible, even if the SAR-derived wind speed has been found to have errors. Then, an attempt is made to use *In-situ* measurements to improve the SAR-derived wind speed fields. As shown in the previous section, the ratio of the SAR-derived mean wind speed to the *In-situ* long-term average is 1.07 and 1.23 at Shirahama and SW-buoy, respectively. Here, the ratios at both Shirahama (1.07) and SW-buoy (1.23) are adopted to correct the tendency of the overestimation. Ratio distributions are estimated by a distance weighted interpolation shown as Figure 4.8. After that, mean wind speed *Vm* and mean energy density *Em* are calculated at all pixels of the SAR image by using the Weibull distribution function. Wind resource maps presented hereinafter show the wind speed after this correction.

Figure 4.9 shows spatial distributions of the SAR-estimated mean wind speed *Vm* and mean wind energy density *Em* at the height of 10 m. It is clearly found that there is a band-like area with strong winds extending from northwest to southwest roughly 20 to 40 km off the coast of Shirahama. Toward the strong wind axis, mean wind speed changes from 3.5 m/s along the coast to nearly 7.5 m/s. The wind energy density ranges from 100 W/m^2 along the coast line to 550 W/m^2 near the strong wind axis. Qualitatively, characteristics of the distributions seem to be reasonable and are similar to the map made with WRF in the previous study (Shimada *et al*., 2011).

Finally, to make wind resource maps at a typical hub height of 80 m, the mesoscale model WRF is used to calculate vertical wind speed ratios between 10 m and 80 m (U80/U10) at each pixel for 104 SAR images. One example of the distribution of the ratio U80/U10 is shown in Figure 4.10. The value normally ranges from nearly 1.0, which corresponds to very unstable atmospheric conditions, to 1.4 in stable conditions. The obtained mean wind speed and mean wind energy density at the height of 80 m are represented in Figure 4.11. It is found that mean wind speed is around 5.0 m/s near the coast of Shirahama, increasing up to nearly 9.0 m/s about 30 km off Shirahama. In terms of mean wind energy density at 80 m height, it is found that the Shirahama offshore platform is located in a weak wind region with wind energy density of 250

W/m^2, and that the maximum wind energy density of more than 800 W/m^2 is located about 30 km to the southwest or west-southwest of the Shirahama offshore platform. The offshore wind resource maps created here will be helpful in the future for development of floating offshore wind farms in the coastal waters.

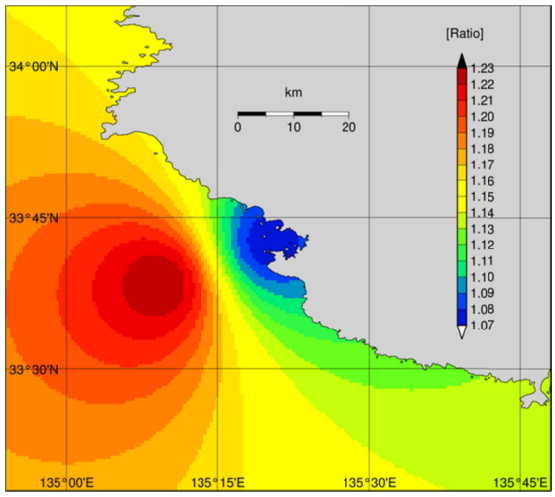

Figure 4.8 Estimated ration distributions between SAR-retrieved wind speed and long-time *In-situ* wind speed based on that at Shirahama and SW-buoy.

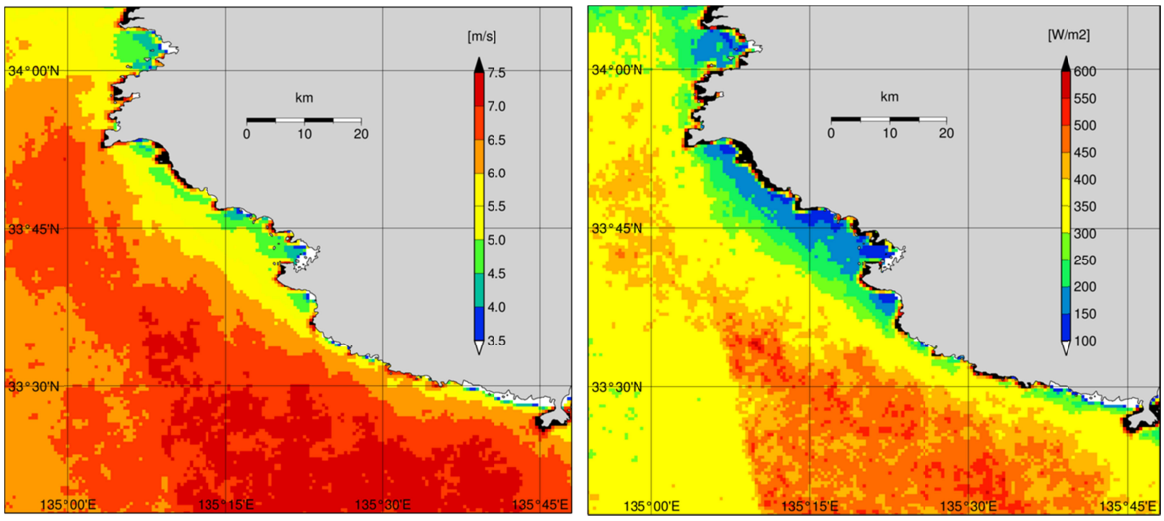

(**a**) Mean wind speed at 10 m (**b**) Mean wind energy density at 10 m

Figure 4.9 Spatial distributions of (**a**) mean wind speed V_m and (**b**) mean wind energy density E_m at 10 m height in the coastal waters off Shirahama.

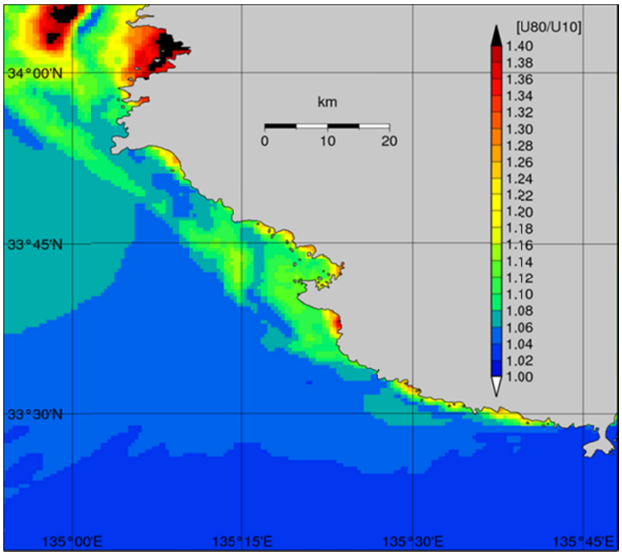

Figure 4.10 An example of the distribution of the ratio U_{80}/U_{10} at 9th September 2005.

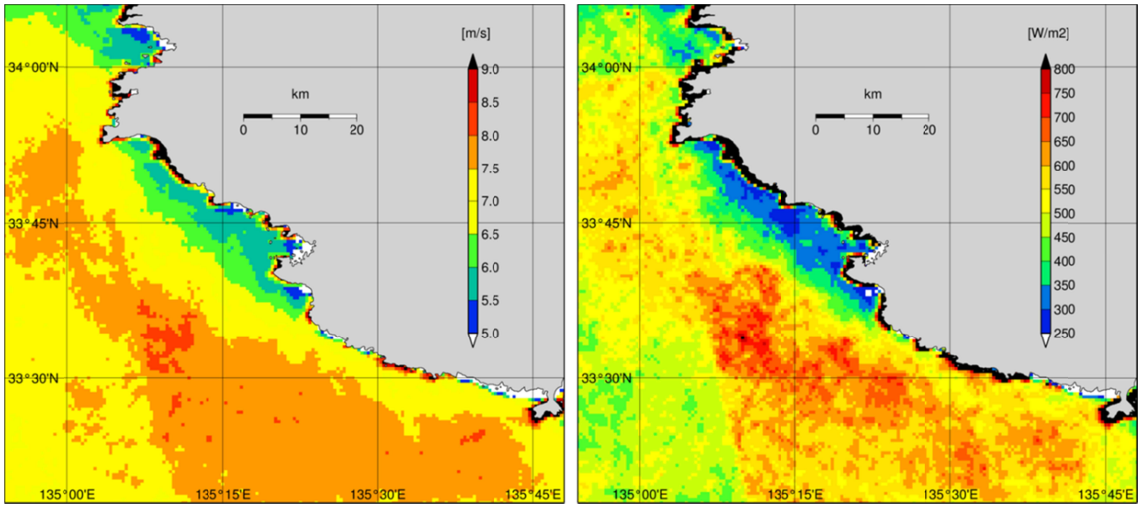

(**a**) Mean wind speed at 80 m (**b**) Mean wind energy density at 80 m

Figure 4.11 Spatial distribution of (**a**) mean wind speed *Vm* and (**b**) mean energy density *Em* at 80 m height in the coastal waters off Shirahama.

4.4 Conclusions

In this study, 104 ENVISAT ASAR images were used to make maps of offshore wind resource in the coastal waters off Shirahama. The geophysical model function CMOD5.N was used to derive wind speed from the SAR images, and the mean wind speed and wind energy density were estimated using the Weibull distribution function. These accuracies were discussed in comparison with *In-situ* measurements from the Shirahama offshore platform (referred to as Shirahama) and the Southwest Wakayama buoy (SW-buoy).

Conclusions in this study are summarized as follows.

1) Compared with *In-situ* measurements at Shirahama, the SAR-derived 10 m-height wind speed had a bias of 0.52 m/s (11 % of *In-situ* mean wind speed) and a RMSE of 2.33 m/s (47 %).
2) The mean wind speed and energy density estimated from SAR images with the Weibull distribution function are 5.45 m/s and 200 W/m2 at Shirahama, and 8.51 m/s and 756 W/m2 at SW-buoy. It is found that the 104 SAR images overestimates the wind resources at both sites, compared to those from long-term *In-situ* wind speed measurements. At Shirahama, SAR overestimates mean wind speed by 7 % compared to the long-term *In-situ* average.
3) In order to obtain more reliable mean wind speed and wind energy density maps, the accuracy of the SAR derived wind speeds was improved by making a long-term bias correction. Then, using the 10 m-height wind speed together with the ratio between 10 m- and 80 m-height wind speeds calculated from the mesoscale meteorological model WRF, mean wind speed and wind energy density maps at 80 m height were made and presented at the end of the paper.

Further works are necessary to increase the accuracy of the maps by combining them with information from remote sensing measurements by satellite-borne scatterometers and radiometers and simulation results from a mesoscale model, as well as by increasing the number of SAR images used in the analysis.

References

Barthelmie, R. J.; Pryor, S. Challenges in predicting power output from offshore wind farms. *Journal of Energy Engineering on Sustainable Energy Systems*, **2012**, *132*, 3. 91-103.

Charnock, H. Wind stress on a water surface. *Quarterly Journal of the Royal Meteorological Society*. **1955**, *81*, 639-640.

Christiansen, M. B.; Koch W.; Horstmann, J.; Hasager C. B.; Nielsen M. Wind resource assessment from C-band SAR. *Remote Sensing of Environment,* **2006**, *105*, 68-81.

Kozai, K.; Ohsawa, T.; Shimada, S.; Takeyama, Y.; Hasager, C. B.; Badger, M. Comparison of Envisat/ASAR-estimated offshore wind resource maps around Shirahama with those from mesoscale models MM5 and WRF. *Proc. European Offshore Wind Conference* **2009a**, PO.131, 7p.

Kozai, K.; Ohsawa, T.; Takahashi, R.; Takeyama, Y. Estimation method for offshore wind energy using synthetic aperture radar and Weibull parameters. *Proc. Nineteenth International Offshore and Polar Engineering Conference* **2009b**, 419-423 (in CD-ROM).

Hersbach, H. Comparison of C-band scatterometer CMOD5.N equivalent neutral winds with ECMWF. *J. Atm. Oceanic Tech.* **2010**, *27*, 721–736.

Hasager, C. B.; Dellwik, E.; Nielsen, M.; Furevik, B. R. Validation of ERS-2 SAR offshore wind-speed maps in the North Sea. *Int. J. Remote Sen*. **2004**, *25*, 3817-3841.

Hasager, C. B.; Badger, M.; Peña, A.; Larsén X. G.; Bingöl, F. SAR-Based Wind Resource Statistics in the Baltic Sea. *Remote Sens.* **2011**, *3*, 117-144.

Liu, W. T.; Katsaros, K. B.; Businger, J. A. Bulk parameterization of air-sea exchanges of heat and water vapor including the molecular constraints at the Interface. *J. Atmos. Sci.***1979**, *36*, 1722–1735.

Liu, W. T.; Tang, W. Equivalent Neutral Wind. JPL publication. **1996**, *96*-17, 8pp.

Shimada, S.; Ohsawa, T. Accuracy and characteristics of offshore wind speeds simulated by WRF. *SOLA* **2011**, *7*, 21-24.

Skamarock, W. C.; Klemp, J. B.; Dudhia, J.; Gill, D. O.; Barker, D. M.; Wang W.; Powers, J. G. A Description of the Advanced Research WRF Version 3. *NCAR Technical Note* **2008**, *TN-468+STR*, 113 pp.

Takeyama, Y.; Ohsawa, T.; Kozai, K.; Hasager, C. B.; Badger, M. Effectiveness of WRF wind direction for retrieving coastal sea surface wind from synthetic aperture radar. WIND ENERGY, **2012**, Early View, DOI:10.1002/we.1526.

Takeyama, Y.; Ohsawa, T.; Kozai, K.; Hasager, C. B.; Badger, M. Comparison of geophysical model functions for SAR wind speed retrieval in Japanese coastal waters, Remote Sensing, **2013**, *5(4)*, 1956-1973, DOI: 10.3390/rs5041956.

Chapter 5

General conclusions

5.1 General conclusions

The wind speed retrieval using ENVISAT synthetic aperture radar (SAR) are attempted with wind directions simulated by the weather research and forecasting model (WRF), in order to evaluate the method for the offshore wind resource assessment.

First, the dissertation discussed the accuracies of geophysical model functions (GMFs) for retrieval of sea surface wind speed from satellite-borne Synthetic Aperture Radar (SAR) images in Japanese coastal waters characterized by short fetches and variable atmospheric stability conditions. *In-situ* observations from two validation sites, Hiratsuka and Shirahama, are used for comparison of the retrieved sea surface wind speeds using CMOD (C-band model) 4, CMOD_IFR2, CMOD5 and CMOD5.N. Of all the geophysical model functions (GMFs), the latest C-band GMF, CMOD5.N, has the smallest bias and root mean square error at both sites. All of the GMFs exhibit a negative bias in the retrieved wind speed. In order to understand the reason for this bias, all SAR-retrieved wind speeds are separated into two categories: onshore wind (blowing from sea to land) and offshore wind (blowing from land to sea). Only offshore winds were found to exhibit the large negative bias, and short fetches from the coastline may be a possible reason for this. Moreover, it is clarified that in both the unstable and stable conditions, CMOD5.N has atmospheric stability effectiveness, and can keep the same accuracy with CMOD5 in the neutral condition. In short, at the moment, CMOD5.N is thought to be the most promising GMF for the SAR wind speed retrieval with the atmospheric stability correction in Japanese coastal waters.

Second, the effectiveness of using the wind direction obtained from the weather research and forecasting (WRF) model are examined in coastal waters adjacent to complex onshore terrain. Wind direction is required as input to the GMF for the retrieval of sea surface wind speed from SAR images. The wind speeds retrieved from 42 ENVISAT ASAR images with WRF wind direction are validated based on *In-situ*

measurements at an offshore platform in Japan. Accuracies are also compared with cases using wind directions: meso-analysis (MANAL) of the Japan Meteorological Agency, the SeaWinds microwave scatterometer on QuikSCAT and National Center for Environmental Prediction (NCEP) final (FNL) operational global analysis data, as well as WRF wind direction. In comparison with the errors of the SAR-retrieved wind speeds obtained using the WRF, MANAL, QuikSCAT and NCEP FNL wind directions, the magnitudes of the errors do not appear to be correlated with the errors of the wind directions themselves. In addition to wind direction, terrain factors are considered to be a main source of error other than wind direction. Focusing on onshore winds (blowing from the sea to land), the root mean square errors on wind speed are found to be 0.75 m/s (*In-situ*), 0.96 m/s (WRF), 1.75 m/s (MANAL), 1.58 m/s (QuikSCAT) and 2.00 m/s (NCEP FNL), respectively, but the uncertainty is of the same order of magnitude because of the low number of cases. These results indicate that although the effectiveness of using the accurate WRF wind direction for the wind retrieval is partly confirmed, further efforts to remove the error due to factors other than wind direction are necessary for more accurate wind retrieval in coastal waters.

Third, offshore wind resource maps for the coastal waters off Shirahama were made based on 104 images of the Advanced Synthetic Aperture Radar (Advanced SAR) onboard the ENVISAT satellite. Wind speed fields were derived from the SAR images with the geophysical model function CMOD5.N. From the obtained wind speeds, mean wind speed and energy density were estimated using the Weibull distribution function. Their accuracies were examined in comparison with *In-situ* measurements from the Shirahama offshore platform and the Southwest Wakayama buoy. It was found that the SAR-derived 10 m-height wind speed had a bias of 0.52 m/s and a RMSE of 2.33 m/s at Shirahama. It was also found that the mean wind speeds estimated from SAR images and the Weibull distribution function were overestimated at both sites. The ratio between SAR-derived and *In-situ* measured mean wind speeds at Shirahama is 1.07 (Shirahama) and 1.23 (SW-buoy), and these values were used for a long-term bias correction in the SAR-derived wind speed. Finally, mean wind speed and wind energy density maps at 80 m height were made based on the corrected SAR-derived 10 m-height wind speeds and the ratio U_{80}/U_{10} calculated from the mesoscale meteorological model WRF.

5.2 Issues in the future

Future works are necessary for the investigation into the effect of the short fetch, causing a negative bias, which shown in Chapters 2 and 3. This negative bias could be more serious in coastal waters than the error originating from wind direction and GMF. Many factors decide a sea surface roughness, and these factors can be affected each other intricately. Many kinds of SAR images with different observation modes should be attempted for next study. Additionally, more number of SAR images may lead more accurate distributions of the mean wind speed and energy density than those in Chapter 4.

Publications

Takeyama, Y.; Ohsawa, T.; Kozai, K.; Hasager, C. B.; Badger, M. Effectiveness of WRF wind direction for retrieving coastal sea surface wind from synthetic aperture radar. WIND ENERGY, **2012**, Early View, DOI:10.1002/we.1526.

Takeyama, Y.; Ohsawa, T.; Kozai, K.; Hasager, C. B.; Badger, M. Comparison of geophysical model functions for SAR wind speed retrieval in Japanese coastal waters, Remote Sensing, **2013**, *5(4)*, 1956-1973, DOI: 10.3390/rs5041956.

Takeyama, Y.; Ohsawa, T.; Yamashita, T.; Kozai K.; Muto, Y.; Baba Y.; Kawaguchi K. Estimation of offshore wind resource in coastal waters off Shirahama using ENVISAT ASAR images, Remote Sensing, **2013**, *5(6)*, 2883-2897, DOI: 10.3390/rs5062883.

Kozai, K.; Ohsawa, T.; Takahashi, R.; Takeyama, Y. Evaluation Method for Offshore Wind Energy Resources Using Scatterometer and Weibull Parameters, Journal of Energy and Power Engineering, **2012**, *6*, 1772-1778.

Kozai K.; Ohsawa, T.; Takahashi, R.; Takeyama, Y. Estimation Method for Offshore Wind Energy using Synthetic Aperture Radar and Weibull Parameters, Proceedings of the Nineteenth International Offshore and Polar Engineering Conference, **2009**,419-423.